Paleoceanography and Paleoclimatology

AGU ADVANCING EARTH AND SPACE SCIENCES

RESEARCH ARTICLE
10.1029/2023PA004609

Special Section:
Illuminating a Warmer World: Insights from the Paleogene

Paleogene Paleohydrology of Ellesmere and Axel Heiberg Islands (Arctic Canada) From Palustrine Carbonates

Ashly B. Padgett[1], Ethan G. Hyland[1], Christopher K. West[2,3], Landon K. Burgener[1,4], David R. Greenwood[5], and James F. Basinger[6]

[1]Department of Marine, Earth & Atmospheric Sciences, North Carolina State University, Raleigh, NC, USA, [2]Department of Earth and Atmospheric Sciences, University of Alberta, Edmonton, AB, Canada, [3]Now at Royal Tyrrell Museum, Drumheller, AB, Canada, [4]Now at Department of Geological Sciences, Brigham Young University, Provo, UT, USA, [5]Department of Biology, Brandon University, Brandon, Manitoba, Canada, [6]Department of Geological Sciences, University of Saskatchewan, Saskatoon, SK, Canada

Abstract Ancient greenhouse periods are useful analogs for predicting effects of anthropogenic climate change on regional and global temperature and precipitation patterns. A paucity of terrestrial data from polar regions during warm episodes challenges our understanding of polar climate responses to natural/anthropogenic change and therefore our ability to predict future changes in precipitation. Ellesmere and Axel Heiberg Islands in the Canadian Arctic preserve terrestrial deposits spanning the late Paleocene to middle Eocene (59–45 Ma). Here we expand on existing regional sedimentology and paleontology through the addition of stable ($\delta^{13}C$, $\delta^{18}O$) and clumped (Δ_{47}) isotope analyses on palustrine carbonates. $\delta^{13}C$ isotope values range from −4.6 to +12.3‰ (VPDB), and $\delta^{18}O$ isotope values range from −23.1 to −15.2‰ (VPDB). Both carbon and oxygen isotope averages decrease with increasing diagenetic alteration. Unusually enriched carbon isotope ($\delta^{13}C$) values suggest that analyzed carbonates experienced repeated dissolution-precipitation enrichment cycles, potentially caused by seasonal fluctuations in water availability resulting in summer carbonate dissolution followed by winter carbonate re-precipitation. Stable isotopes suggest some degree of precipitation seasonality or reduction in winter water availability in the Canadian Arctic during the Paleogene. Clumped (Δ_{47}) temperature estimates range from 52 to 121°C and indicate low temperature solid-state reordering of micritic samples and diagenetic recrystallization in sparry samples. Average temperatures agree with vitrinite reflectance data for Eureka Sound Group and underlying sediments, highlighting structural complexity across the region. Broadly, combined stable and clumped isotope data from carbonates in complex systems are effective for describing both paleoclimatic and post-burial conditions.

Plain Language Summary Paleogene paleohydrology in Arctic Canada has been a question of much debate in recent years, with competing ideas about conditions characterized as either "polar monsoon" or "ever-wet" regimes. Proxy records from Ellesmere and Axel Heiberg islands have been central to this debate, but complex stratigraphy and burial histories have hampered a resolution. Here we employ a combined carbonate isotope ($\delta^{13}C$, $\delta^{18}O$, Δ_{47}) approach to disentangle paleoclimate and diagenetic signals. Using palustrine carbonates (which host previously evaluated paleobotanical remains) within a new stratigraphic framework, we demonstrate that $\delta^{13}C$ and $\delta^{18}O$ values from primary-fabric samples indicate a distinct, but non-monsoonal hydrologic seasonality during the late Paleocene/early Eocene. We also demonstrate that Δ_{47} temperatures reflect both shallow burial reordering and more intense remineralization, which are consistent with vitrinite reflectance studies showing variable deformation and geothermal gradients in the Sverdrup Basin. This combined isotopic approach is novel in the region, and can be applied to other regions of interest in deep time.

Key Points:

- Combined carbonate isotope approach disentangles paleoclimate/diagenesis despite complex environmental histories on Ellesmere/Axel Heiberg
- Carbon and oxygen isotope values highlight hydrologic seasonality in the Arctic during the Paleogene
- Temperatures from carbonate clumped isotopes are consistent with vitrinite reflectance burial temperature, suggesting variable deformation

Correspondence to:
E. G. Hyland,
ehyland@ncsu.edu

Citation:
Padgett, A. B., Hyland, E. G., West, C. K., Burgener, L. K., Greenwood, D. R., & Basinger, J. F. (2023). Paleogene paleohydrology of Ellesmere and Axel Heiberg Islands (Arctic Canada) from palustrine carbonates. *Paleoceanography and Paleoclimatology*, *38*, e2023PA004609. https://doi.org/10.1029/2023PA004609

Received 9 JAN 2023
Accepted 25 SEP 2023

Author Contributions:

Conceptualization: Ethan G. Hyland
Data curation: Ashly B. Padgett, Ethan G. Hyland
Formal analysis: Ashly B. Padgett, Ethan G. Hyland, Landon K. Burgener
Funding acquisition: Ethan G. Hyland, David R. Greenwood, James F. Basinger
Investigation: Ashly B. Padgett, Ethan G. Hyland
Methodology: Ethan G. Hyland, Landon K. Burgener
Project Administration: Ethan G. Hyland

1. Introduction

Predicting future changes to global precipitation patterns is critical for global food security, water resource management, and extreme event preparedness (IPCC, 2021). However, current precipitation predictions vary significantly among climate models due to their distinct parameters (e.g., RCP Scenarios; IPCC, 2021; USGCRP, 2018). A better understanding of precipitation dynamics during past greenhouse periods is required to improve future precipitation simulations (QDRR, 2010; Tierney et al., 2020). As the polar regions are particularly responsive to global climate change, improvement to our overall understanding of past high latitude hydrological

Resources: Ethan G. Hyland, Christopher K. West, David R. Greenwood, James F. Basinger
Software: Landon K. Burgener
Supervision: Ethan G. Hyland
Visualization: Landon K. Burgener
Writing – original draft: Ashly B. Padgett
Writing – review & editing: Ashly B. Padgett, Ethan G. Hyland, Christopher K. West, Landon K. Burgener, David R. Greenwood, James F. Basinger

regimes contributes to models of both regional and global paleohydrology and to our capacity to predict anthropogenic change.

Proxy records from past greenhouse periods exist for some regions and time periods; however, the majority of climate records currently available from Mesozoic and Paleogene warm periods are from marine environments, which may temporally lag corresponding terrestrial events (Mix & Ruddiman, 1984), and typically show diminished responses to warming (Diffenbaugh & Field, 2013). Modern climate monitoring and simulations of future warming have also shown that high-latitude regions respond dramatically to rapid warming events and can further influence the global climate (USGCRP, 2018), highlighting the need to increase our understanding of high-latitude climate dynamics. Some terrestrial proxy records from greenhouse periods exist for the Arctic (e.g., Greenwood et al., 2010; Guemas et al., 2013; Salpin et al., 2019; Suan et al., 2017; Sunderlin et al., 2011; West et al., 2015, 2020; Willard et al., 2019; Zimov et al., 2006) and southern high latitudes (e.g., Carpenter et al., 2012; Contreras et al., 2013; Francis & Poole, 2002; Ivany et al., 2011; Jacques et al., 2014; Pross et al., 2012; Reguero et al., 2002). Nevertheless, the amount of data available for terrestrial areas is comparatively low and often complicated for these crucial regions (e.g., Huber & Caballero, 2011); therefore, expanding our inventory of high-latitude terrestrial proxy records will continue to improve our understanding of the function of the hydrologic cycle during past greenhouse periods (e.g., Carmichael et al., 2016).

Accessible land area in polar regions is limited and deep-time archives are often obscured by subsequent deformation, making it difficult to unravel environmental histories. In particular, the Canadian Arctic has experienced tectonic reorganization since the Mesozoic, including significant burial and exhumation of certain terranes (e.g., Ricketts & Stephenson, 1994; Embry & Beauchamp, 2008; von Gosen et al., 2019). Previous studies found extension and rapid subsidence of the eastern part of the region (Sverdrup Basin), which resulted in increased sedimentation between the Late Cretaceous and the middle Eocene. This period of deposition was followed by regional uplift and denudation from the middle Eocene onward (Figure 1; e.g., Dewing & Obermajer, 2011; Dewing & Sanei, 2009; Embry & Beauchamp, 2008; von Gosen et al., 2019). Understanding such complex sedimentary basin dynamics can be important for interpreting samples within the context of their tectonic histories and evaluating robustness of paleoclimate records.

One way to address both climate and tectonic evolution questions in complex settings like the Canadian Arctic Archipelago is to employ a combination of traditional stable and novel clumped isotope systems to identify pre- and post-burial influences on carbonate rocks, and to thereby separate paleoclimatic from burial/deformation signals (e.g., Parrish et al., 2018; Winkelstern & Lohmann, 2016). The main objectives of this study are to use the carbon, oxygen, and clumped isotopic compositions of terrestrial carbonates to determine (a) if the Paleogene Arctic hydrologic system experienced some form of seasonality or periodicity in water availability, and (b) if paleoclimate information can be disentangled from signals generated by burial and subsequent carbonate alteration using a multi-proxy approach. Specifically, we analyze both the (relatively burial-insensitive) stable and (relatively burial-sensitive) clumped isotope compositions of palustrine carbonates from Ellesmere and Axel Heiberg islands (Nunavut, Canada) and use these complex data sets to provide new constraints on both Arctic paleohydrology and burial/deformation in the eastern Sverdrup Basin.

2. Background

2.1. Paleogene Arctic Climate

The modern Canadian Arctic environment is a polar desert, and is typified by a cold, dry climate inhabited by cold-adapted flora and fauna. However, during the early Paleogene, the Canadian Arctic was home to forests dominated by temperate deciduous hardwoods, conifers, and ferns (McIver & Basinger, 1999; West et al., 2019), and a diverse polar fauna consisting of thermophilic animals such alligators, snakes, turtles, and tapirs (Eberle et al., 2014; Eberle & Greenwood, 2012; Estes & Hutchison, 1980).

The Canadian Arctic region during the early Paleogene was broadly temperate and wet (Eldrett et al., 2014; Greenwood et al., 2010; West et al., 2020), and previous paleobotanical studies have indicated these regions experienced high mean annual precipitation (>>150 cm/year), mesothermal conditions (mean annual temperature (MAT) ~12–15°C), and moderate winter temperatures (Cold month mean temperature (CMMT) > 0°C) (West et al., 2015, 2020). The forests of the Canadian Arctic grew during a warm greenhouse interval when global temperatures were much higher than modern, and the global climate system was episodically punctuated by short-lived transient hyperthermal events (McInerney & Wing, 2011; Sluijs et al., 2009; Zachos et al., 2008).

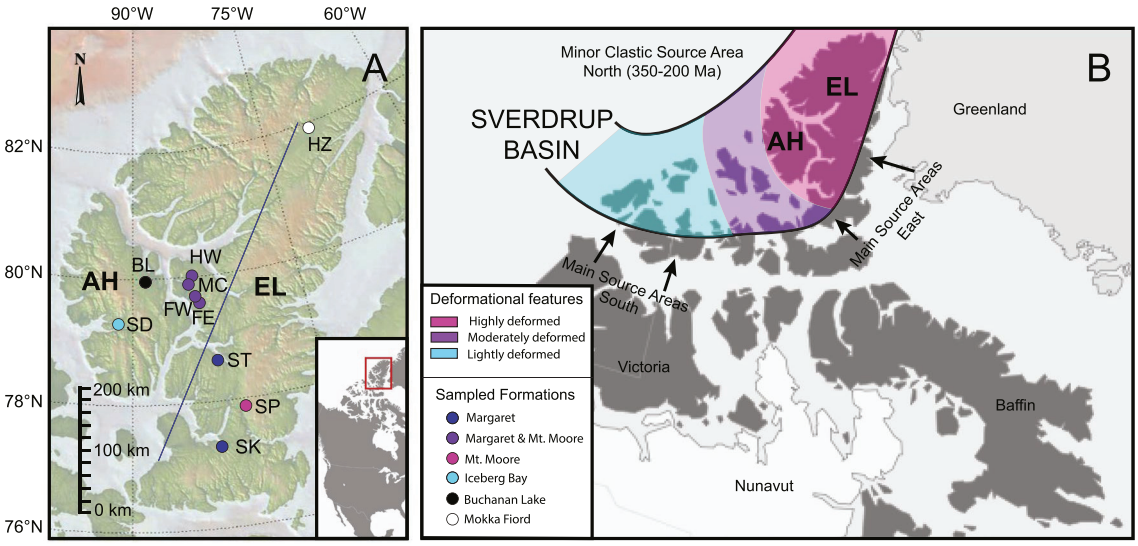

Figure 1. Maps of Ellesmere (EL) and Axel Heiberg (AH) islands. (a) Topographic map for Ellesmere (EL) and Axel Heiberg (AH) islands. Axel Heiberg Island contains the sample locations: Buchanan Lake (BL) and Strand Fiord (SD). Ellesmere Island contains the sample locations: Lake Hazen (HZ), Hot Weather Creek (HW), Mosquito Creek (MC), Fosheim Anticline West (FW), Fosheim Anticline East (FE), Strathcona Fiord (ST), Split Lake (SP), and Stenkul Fiord (SK). Topographic data from GeoMapApp (Ryan et al., 2009). Blue line in Panel A indicates NE-SW transect shown in Figure 6. (b) Placement of the Sverdrup Basin across the Canadian Arctic Archipelago, with sediment source areas indicated. Deformation regimes in the Sverdrup Basin include "highly deformed" with thrust faults and significant folding; "moderately deformed" with folding and salt domes; and "lightly deformed" where there is very mild deformation with broad folds (e.g., Embry & Beauchamp, 2008).

These intense episodes of global warming are considered to be some of the most abrupt and dramatic climatic warming events of the entire Cenozoic and represent some of the warmest intervals of the last 66 million years (McInerney & Wing, 2011; Westerhold et al., 2020; Zachos et al., 2008). Perhaps the best studied and most dramatic of these events is the Paleocene-Eocene Thermal Maximum (PETM), which was characterized by a large negative carbon isotope excursion (>4‰ in terrestrial archives) and a subsequent global temperature increase of approximately 5–8°C in ≤20ky (e.g., Eldrett et al., 2014; Sluijs et al., 2009; Zachos et al., 2008).

The PETM and other Paleogene warming events not only increased mean global temperatures, but also affected the global hydrological system, including precipitation intensity and distribution (Hyland & Sheldon, 2013; Hyland et al., 2017; Krishnan et al., 2014; Pagani et al., 2006; Westerhold et al., 2020; Zachos et al., 2008). The hydrological response on a regional scale was complex, with shifts to wetter or drier climates recorded in different regions (Zachos et al., 2008). Mid-latitude environments that were warm and wet were marked by a decrease in precipitation that preceded or occurred during the PETM (Garel et al., 2013; Kraus et al., 2013; Wing et al., 2005). However, proxy evidence from wet-temperate high-latitude environments such as the Canadian Arctic, Spitzbergen and North Sea, reveal positive increases to both temperature and precipitation (Eldrett et al., 2014; Greenwood et al., 2010; Uhl et al., 2007; West et al., 2015, 2020).

The seasonality of precipitation, or the availability of water, remain important aspects of paleohydrological research, particularly during greenhouse climates. Recently, global climate models have reconstructed precipitation patterns for the early Eocene and identified the existence of robust seasonal precipitation patterns within much of the middle and lower latitudes (e.g., Huber & Goldner, 2012), whereas the high latitudes were instead modeled as having a low precipitation seasonality, or considered "ever-wet" (Carmichael et al., 2016; Huber & Goldner, 2012). Leaf physiognomic analyses from Stenkul Fiord (Ellesmere Island) also showed that estimates of mean annual precipitation and growing season precipitation indicated a more even distribution of annual precipitation (West et al., 2015). In contrast, high-resolution carbon isotope analyses of fossil wood from Stenkul Fiord showed a summer peak in precipitation and characterized the region as "monsoonal" (Schubert et al., 2012).

2.2. Geologic Setting

Ellesmere and Axel Heiberg islands are located in the Canadian Arctic Archipelago within the Nunavut territory of Canada (Figure 1). These islands are at present positioned from 77°N to 82°N, and were approximately 2°

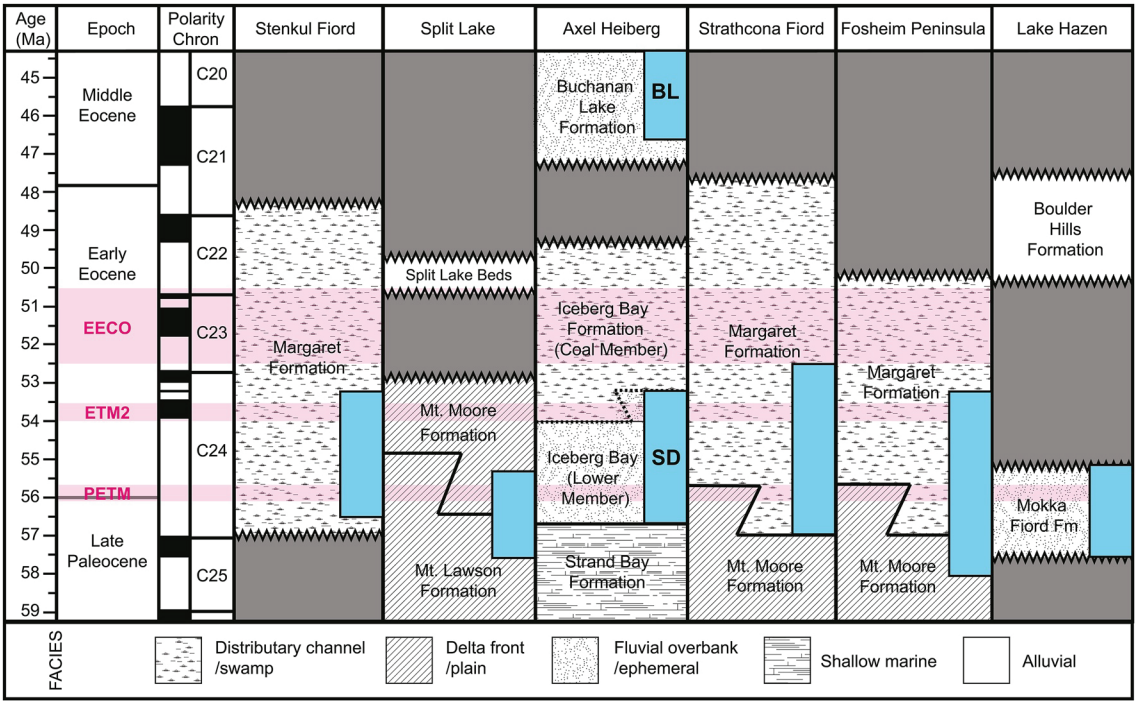

Figure 2. Simplified stratigraphic column of relevant Eureka Sound Group formations with sample locations. Approximate sampling intervals indicated by colored bars (blue) for each locality, and include: Stenkul Fiord (US435, US436, US438), Split Lake (US444), Axel Heiberg (Strand Fiord [SD], US176; Buchanan Lake [BL], US119), Strathcona Fiord (US422), Fosheim Peninsula (Hot Weather Creek, US107, US108; Mosquito Creek, US196; Fosheim Anticline, US111, US191, US251), and Lake Hazen (US261). Pink shaded regions indicate major climatic events (e.g., Westerhold et al., 2020), base column and depositional environments adapted from West et al. (2019) and Miall (1986).

further south (75˚N to 80˚N) from 66 to 40 Ma (Irving & Wynne, 1991; Jahren, 2007; West et al., 2019). At these latitudes, the islands experienced continuous darkness during winter and continuous light during summer, with short spring and fall transitions. The Sverdrup Basin (approximately 1,000 km by 350 km) spans the northern Canadian Arctic Archipelago, including Axel Heiberg Island and most of Ellesmere Island, and contains up to 13,000 m of strata of Paleozoic to Cenozoic age (Figure 1; Núñez-Betelu et al., 1994). The clastic sediments that were deposited in the Sverdrup Basin during the Paleocene and Eocene comprise the Eureka Sound Group (ESG). Our examined suite of samples is from the ESG and were deposited and deformed during burial and uplift phases of the Eurekan Orogeny (Dewing & Obermajer, 2011). As a result, many of the carbonates of the ESG experienced deformation and heating, which is important context when applying the isotopic data from these ESG carbonates to climate or burial history reconstructions.

2.3. Eureka Sound Group

The stratigraphy of the ESG was recently reviewed by West et al. (2019), which simplifies various nomenclature conventions and offers a comprehensive overview of the refined stratigraphy. The late Paleocene to early Eocene samples analyzed here are from the Mount Moore, Margaret, and Mokka Fiord Formations. Outcrops of these formations are present in many locations across Ellesmere and Axel Heiberg islands, with ages constrained by litho-stratigraphy, biostratigraphy, magnetostratigraphy, and U-Pb zircon dating (Figure 2; Eberle & Greenwood, 2012; Harrison et al., 1999; Miall, 1986; Reinhardt et al., 2013; Ricketts, 1986; Ricketts & Stephenson, 1994; Sudermann et al., 2021; Tauxe & Clark, 1987; von Gosen et al., 2019; West et al., 1977, 1981, 2019). Because units are diachronous based on the location and degree of tectonic denudation experienced, a more precise age control beyond late Paleocene to early Eocene cannot be defined and samples could have varying or overlapping ages between 59 and 48 Ma (Figure 2). Unlike the other samples, the Buchanan Lake Formation on Axel Heiberg is considered middle Eocene, with an age approximation of about 45 Ma (Ricketts & McIntyre, 1986; Ricketts & Stephenson, 1994; Eberle & Storer, 1999; Eberle & Greenwood, 2012; Figure 2). Overall, the lack of a composite stratigraphy for the ESG and these sites specifically means we are unable to place our measured samples

stratigraphically or chronologically with precision, and therefore choose to group them by larger time period (late Paleocene/early Eocene vs. middle Eocene).

On Ellesmere and Axel Heiberg islands, ESG strata from the late Paleocene to middle Eocene are dominated by fluvio-deltaic, floodplain, and paludal deposits (Miall, 1986; Ricketts, 1986; Ricketts & Stephenson, 1994). Specifically, the Mount Moore/Mount Lawson Formation consists primarily of interbedded brown sand and siltstones with some plant fossils, defined as delta front/plain facies; the Margaret Formation consists of siltstones, mudstones, and coals with abundant plant fossils, defined as distributary channel/swamp facies; the Iceberg Bay Formation consists of fine sandstone channels and calcareous brown shales with thin coal seams, defined as fluvial overbank or ephemeral fluvial facies; the Buchanan Lake Formation consists of carbonaceous mudstones and thin coals, defined as fluvial overbank or ephemeral fluvial facies; and the Mokka Fjord Formation consists of silty mudstones, carbonaceous mudstones, and coals, defined as fluvial overbank facies (Figure 2; Miall, 1986). In each case, environmental interpretations of our analyzed carbonate mudstone samples where leaf fossils were recovered suggest our samples were palustrine and deposited in wet floodplain/swamp or overbank/crevasse splay deposit facies, which may have been alternately seasonally inundated and subjected to pedogenic processes (Eberle & Greenwood, 2012; West et al., 2019).

3. Materials and Methods

3.1. Sample Collection and Evaluation

Samples were collected from paleobotanical surface quarries during multiple field seasons (1982–2004). Carbonates were associated with described fossil leaf assemblages to assign stratigraphic positions within the ESG (e.g., Eberle & Greenwood, 2012; Greenwood et al., 2010; West et al., 2015, 2019, 2020). Samples were prepared and cataloged for collections purposes within the University of Saskatchewan's Paleobotanical Collection (USPC), and a suite of 14 palustrine carbonate rocks were selected from the collection based on primary carbonate textures and geographic distribution within the ESG. Samples were selected from seven locations on Ellesmere Island (Lake Hazen, Mosquito Creek, Hot Weather Creek, Fosheim Anticline, Strathcona Fiord, Split Lake, and Stenkul Fiord) and two locations on Axel Heiberg Island (Buchanan Lake and Strand Fiord). Hand samples were cut with a rock saw to produce standard billets and sent to Wagner Petrographic for thin section preparation. Thin sections were examined under plain and polarized light on a petrographic microscope to estimate spar and micrite ratios and evaluate carbonate fabric.

To quantitatively classify samples into textural categories, a scaled percentage of spar coverage was calculated for each thin section. This approach factored in both spar coverage and crystal size, as some slides had large spar crystals and others had "micro"-spar, and provided an additional numerical value to compare between percentages of spar versus micrite and categorical designations. A random walk of 60 spar crystals was taken for each slide to approximate an average spar crystal length and width. Spar crystal dimensions were applied into an ellipse formula to calculate average spar area, which was multiplied by a general approximation of percent spar coverage for each slide. That product was then divided by a baseline of maximum crystallinity in μm^2 (the largest average spar size at 100% coverage on the slide) to produce a scaled percentage of spar coverage. Based on the order of magnitude (0.000X, 0.00X, 0.0X, 0.X) of the scaled percentage of spar coverage (referred to herein as the Visual Alteration Coefficient [VAC]), samples were classified as micritic (Mic), sub-micritic (SMic), microspar (MSp), and sparry (Spar) respectively (Figure 3). This method quantifies visual evidence of diagenetic alteration, but it is important to note that this VAC works on the uncertain assumption that spar size and the ratio of spar-to-micrite would have an equal effect on the scaled percentage.

3.2. Isotope Analyses

Carbonate clumped isotope thermometry is based on preferential bonding of heavier isotopes of carbon (^{13}C) and oxygen (^{18}O) together within carbonate minerals (Eiler, 2007, 2011). The heavier isotopes approach a stochastic abundance at 1000°C, while at cooler temperatures heavier isotopes preferentially "clump" (Eiler, 2007). The proportion of multiply-substituted isotopologues in a carbonate sample can be used to estimate carbonate mineral growth temperatures, and constrain paleoclimatic, paleoenvironmental, and diagenetic conditions during carbonate formation (e.g., Bristow et al., 2011; Eiler, 2011; Ferry et al., 2011; Huntington et al., 2011). Carbonates were microsampled in at least two separate locations within each billet using a carbide steel burr drill

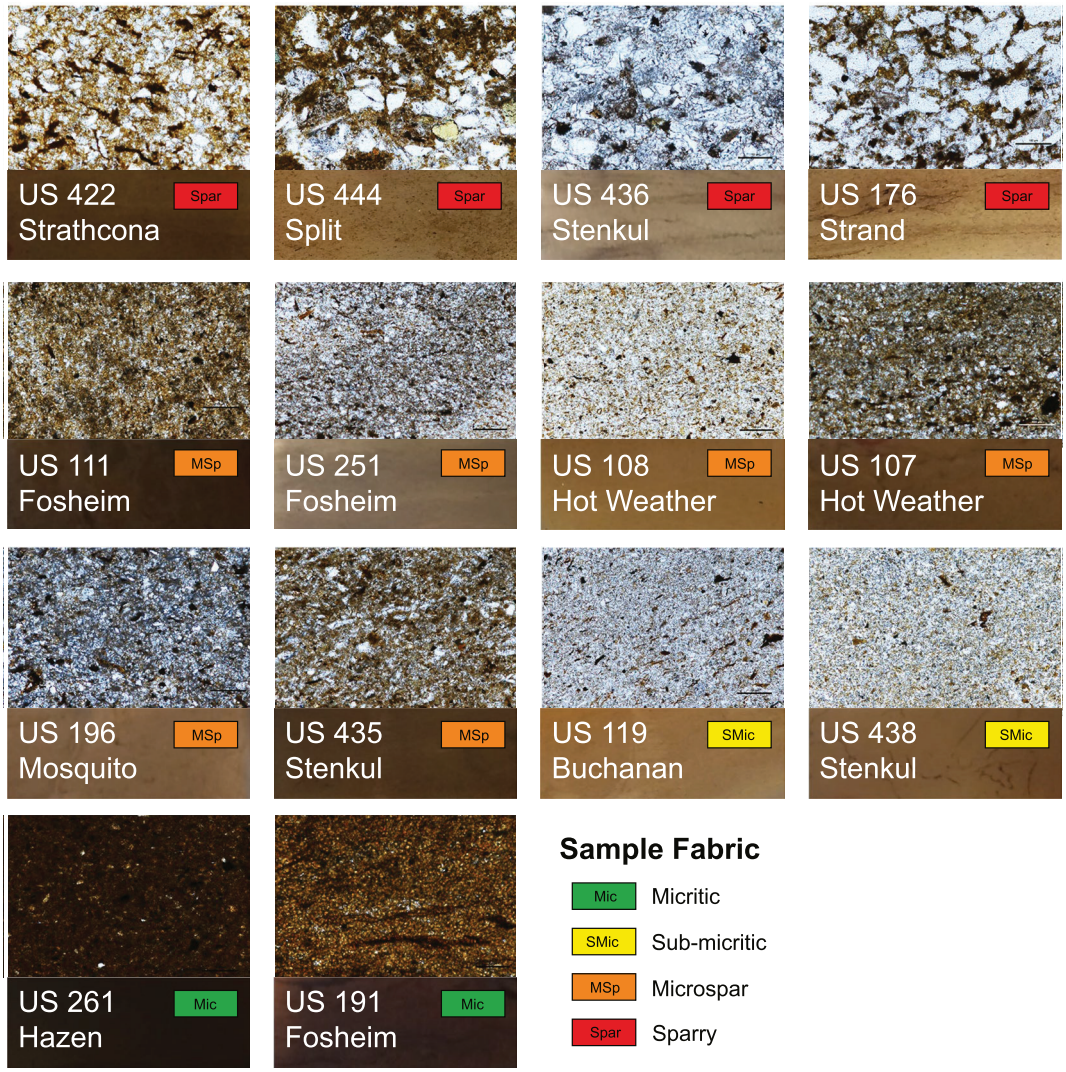

Figure 3. Plain light images of thin sections showing example fabrics. Microscope image size is 700 μm by 400 μm in each case, and images approximate average fabric for the selected samples with no specific features highlighted. Sample numbers/locality names correspond to locations indicated in Figures 1 and 2.

bit on a Stoelting handheld micro drill, and additionally subsampled from a different location on the hand sample. Powdered samples were analyzed for stable ($\delta^{18}O$, $\delta^{13}C$) and clumped (Δ_{47}) isotopes at the Paleo^3 Laboratory at North Carolina State University. Samples were processed in a Nu Carb Automated Carbonate on-line preparation system at 70°C. Powdered samples (stable 500–700 μg, clumped average 2200 μg) were digested with phosphoric acid (specific gravity 1.94–1.96), and resultant CO_2 was cryogenically separated and passed through a Porapak Q trap held at −28°C. The evolved CO_2 was stored in the dual inlet alongside a CO_2 working gas (compositions: $\delta^{13}C = 4.485$, $\delta^{18}O = -2.450$).

Sample $\delta^{18}O$, $\delta^{13}C$, and Δ_{47} values were measured on a Nu Perspective Isotope Ratio Mass Spectrometer configured to measure m/z ratios for masses 44–49, and are reported relative to the standard Vienna-Pee Dee Belemnite (VPDB) and the Intercarb-Carbon Dioxide Equilibrium Scale (I-CDES; Bernasconi et al., 2021). Two solid standards were run before and after each set of eight unknown carbonate samples. $\delta^{18}O$ and $\delta^{13}C$ output was referenced to IAEA standards C-1 and NBS-18; Δ_{47} output was referenced to ETH solid standards (ETH-1, ETH-2, ETH-3, ETH-4) (Bernasconi et al., 2021). Data were processed using Easotope software (John & Bowen, 2016), using the Brand et al. (2010) ^{17}O correction parameters (Daëron et al., 2016; Schauer et al., 2016) and corrected with a 70°C calcite acid fractionation of 0.066 (Petersen et al., 2019). Replicates with Δ_{48} offset values exceeding ±2‰ were rejected due to potential contamination by organics or hydrocarbons (Guo & Eiler, 2007; Huntington

et al., 2009). The Pierce Outlier test was used to remove statistical outliers from the stable and clumped output (Burgener et al., 2016; Huntington et al., 2009), the standard error was measured based on a 95% confidence interval, and T(Δ_{47}) were calculated using the Petersen et al. (2019) calibration.

Here, calcite $\delta^{18}O$ ($\delta^{18}O_{calcite}$) values were also converted to $\delta^{18}O_{sw}$ using the Kim and O'Neil (1997) calcite-water isotope fractionation equation, which describes the relationship between the oxygen isotope value of a carbonate mineral ($\delta^{18}O_{calcite}$), the oxygen isotope value of the source water in which the calcite formed ($\delta^{18}O_{sw}$), and temperature (T) (Kim & O'Neil, 1997).

$$\delta^{18}O_{calcite} \approx \delta^{18}O_{sw} + 18.03 * \left(10^3 / T\right) + 32.42 \quad (1)$$

4. Results

4.1. Sample Descriptions

Hand samples are tan to dark brown, fine-grained, and well-indurated minor carbonate rocks (8%–45% $CaCO_3$). Most hand samples are massive (no lamination to rare and very fine lamination) and have significant disseminated fine organic debris and variably abundant leaf fossils throughout. Samples lack specific pedogenic and surface alteration features, and primary micrite is mixed with recrystallized phases. In thin section, samples contain no obvious biological (e.g., shell fragments, microbial coatings) or detrital grains, nor do they exhibit unique textural features beyond simple lamination and spar growth (Figure 3). Samples appear to be exclusively calcite and have two clear generations of carbonate formation (first generation micrite and spar recrystallization) but vary in the degree of diagenetic alteration (Figure 3). Sparry samples US422, US444, US436, and US176 have occasional organics and coarse spar crystals (average spar length ~55 μm, large spar crystal length >100 μm) distributed throughout the thin section. Microspar samples US111, US107, US196, and US435 have moderate to high organic content with close to an equal ratio of microspar (average spar length ~15 μm) to micrite and organics. Microspar samples US251 and US108 have low organic content and significant spar (average spar length ~10 μm) distribution throughout the samples. Sub-micritic samples US119 and US438 have low organic content and fine spar (average spar length ~7 μm) interspersed with micrite. Micritic samples US261 and US191 have very high organic content and very low spar presence (average spar length <7 μm).

4.2. Isotope Analyses

$\delta^{13}C$ isotope values range from −4.6 to +12.3‰ (VPDB) and $\delta^{18}O$ isotope values range from −23.1 to −15.2‰ (VPDB). Samples within each fabric type (micritic, sub-micritic, microspar, and sparry) have $\delta^{13}C$ averages of 9.8, 4.5, 3.4, 2.0‰, respectively. Samples within each fabric type have $\delta^{18}O$ averages of −17.2‰, −17.8‰, −18.0‰, −18.9‰, respectively (Figure 4; Table 1). Δ_{47} values range from 0.505 to 0.621‰ (I-CDES) with resulting temperature estimates (T[Δ_{47}]) from 52 to 121°C. Temperatures were on average higher for samples experiencing more significant alteration (higher VAC; Figure 4; Table 1).

5. Discussion

5.1. Sample Interpretation

Evaluation of the hand-samples and thin-sections provides evidence of the pedogenic, groundwater, and subsequent burial processes that impacted sample $\delta^{13}C$, $\delta^{18}O$, and Δ_{47} values. High fossil leaf preservation and lack of calcrete characteristics and surface alteration features (including desiccation features, modifications associated with roots and soil organisms, and the remobilization of carbonate and iron) serve as evidence that samples are less-developed palustrine carbonates that underwent minimal pedogenic development (Alonso-Zarza, 2003; Freytet, 1984; Marty & Meyer, 2006). Well-indurated hand samples indicate that primary micrite is mixed with recrystallized phases, and samples may have undergone varying degrees of aggrading neomorphism from pore fluid interactions (Alonso-Zarza et al., 2006).

In thin section, samples display two dominant generations of carbonate formation (first generation micrite and spar recrystallization) but vary in the degree of secondary diagenetic alteration. Consistent coarse spar distribution and equant/elongate crystal formation within microspar and sparry sample thin sections suggest they

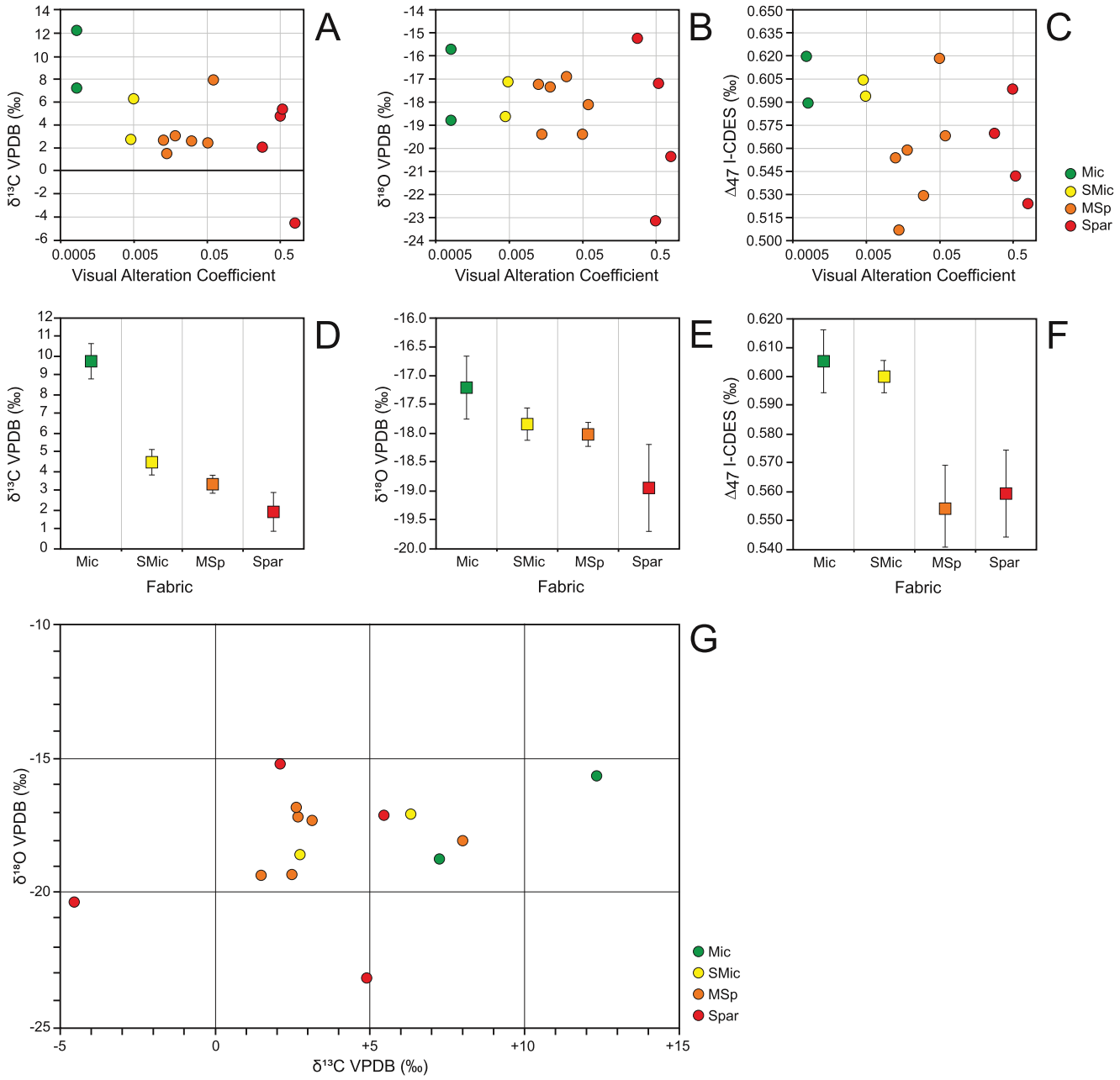

Figure 4. Stable and clumped isotope results. Visual Alteration Coefficient versus carbon isotope composition (a), oxygen isotope composition (b), and clumped isotope composition (c). Isotopic averages for each fabric type with standard deviation bars (d–f). Carbon-oxygen isotope crossplot (g).

experienced burial diagenesis. The scaled percentage of spar coverage was used to evaluate the isotope data within respective fabric categories (Mic, SMic, MSp, Spar). By using a numerical classification scheme, changes in primary carbonate fabrics can be more accurately quantified to indicate how much alteration occurred due to burial and reheating.

5.2. Burial and Deformation in the Sverdrup Basin

5.2.1. Stable Isotopes and Burial Diagenesis

In addition to the environmental processes described below (see Section 5.3), the $\delta^{13}C$ and $\delta^{18}O$ values of some of our samples are influenced by diagenesis related to post-depositional burial. In order of increasing diagenetic

Table 1
Stable and Clumped Isotope Data Summary

Sample	Location	VAC	Fabric	Replicates (n =)	Avg $\delta^{13}C$	SE ($\delta^{13}C$)	Avg $\delta^{18}O$	SE ($\delta^{18}O$)	Avg Δ_{47}	SE (Δ_{47})	Temp (°C)	Temp error (±°C)
US119	BL	0.0045	SMic	7	2.73	0.099	−18.61	0.271	0.604	0.018	59.6	6
US444	SP	0.5	Spar	6	4.86	0.070	−23.12	0.140	0.599	0.026	62.2	9
US107	HW	0.03	MSp	7	2.60	0.097	−16.86	0.139	0.529	0.018	102.5	6
US108	HW	0.018	MSp	9	3.10	0.047	−17.31	0.035	0.558	0.033	84.2	10
US435	SK	0.06	MSp	8	7.95	0.114	−18.07	0.088	0.567	0.016	79.0	5
US436	SK	0.54	Spar	6	5.42	0.574	−17.14	0.398	0.542	0.012	94.2	4
US438	SK	0.0048	SMic	9	6.31	0.046	−17.06	0.161	0.596	0.021	63.2	7
US261	HZ	0.0008	Mic	7	12.32	0.094	−15.67	0.052	0.621	0.032	51.6	10
US191	FW	0.0008	Mic	8	7.23	0.130	−18.74	0.053	0.589	0.025	66.8	9
US111	FW	0.0125	MSp	7	2.68	0.121	−17.17	0.227	0.555	0.021	86.0	7
US251	FE	0.014	MSp	6	1.47	0.078	−19.36	0.196	0.505	0.03	120.6	10
US422	ST	0.28	Spar	8	2.09	0.024	−15.21	0.260	0.570	0.02	77.4	7
US196	MC	0.05	MSp	9	2.45	0.029	−19.33	0.187	0.618	0.023	52.9	8
US176	SD	0.8	Spar	5	−4.56	0.166	−20.32	0.803	0.525	0.001	105.6	3

Note. Abbreviations for locations as in Figure 1, and fabrics as in Figure 3. Δ_{47} values reported in I-CDES, corrected to 90°C.

alteration, the mean $\delta^{13}C$ values for our samples decrease from 9.8‰ for Mic, 4.5‰ for SMic, 3.4‰ for MSp, and 2.0‰ for Spar, and mean $\delta^{18}O$ values decreased from −17.2‰ for Mic, −17.8‰ for SMic, −18.0‰ for MSp, and −18.9‰ for Spar (Figure 4). Both the mean $\delta^{13}C$ and $\delta^{18}O$ values display a marked overall decrease with increased alteration, showing a transition from primary micrite (original source water composition) to increasing proportions of secondary calcite spar (burial fluid composition) (Dunagan & Turner, 2004; Tandon & Andrews, 2001). Variation in $\delta^{13}C$ within each respective alteration class likely reflects an influx of depleted carbon sourced from hydrothermal fluids equilibrated with more deeply buried carbonates; for example, deeper Permian-Triassic carbonates from these locations have $\delta^{13}C_{org}$ of about −25 to −30‰ (Grasby & Beauchamp, 2008), and carbonates precipitated from groundwater equilibrated with these deeper rocks would have $\delta^{13}C$ values of about −10 to −15‰ (Oehlert & Swart, 2014).

Gradual decreases in $\delta^{18}O$ from micritic to secondary calcite samples likely reflect the temperature-dependent fractionation of $\delta^{18}O$ as the spar crystallized out of hot diagenetic fluids with a distinct composition (Kim & O'Neil, 1997; Tandon & Andrews, 2001). Using known temperature-dependent fractionation relationships between the $\delta^{18}O$ of calcite and source fluids (Cerling & Quade, 1993; Kim & O'Neil, 1997), we can use the methods shown above (Section 3.2) for microspar and spar samples. By substituting actual clumped isotope temperatures ($T[\Delta_{47}]$) for an assumed environmental temperature (cf., Section 5.3.2), we can calculate source water ($\delta^{18}O_{sw}$) values for these spar-formation fluids, which range from −2.1 to −5.2‰ (VSMOW). These values are significantly enriched in ^{18}O relative to estimated environmental/meteoric waters for the region during the Paleogene (e.g., Jahren & Sternberg, 2008; Tripati et al., 2001), suggesting source fluids for spar components were either dominantly metamorphic (e.g., Hoefs, 2021) or were hydrothermal fluids undergoing significant water-rock interactions in the subsurface (see above; see also Ferry & Gerdes, 1998; Taylor & Epstein, 1962). Localized impacts of hydrothermal fluids in these sediments are unsurprising, given the regional gradient in deformation across the basin (e.g., Figure 1b; Embry & Beauchamp, 2008).

5.2.2. Carbonate Δ_{47} and Burial Diagenesis

Δ_{47} ratios of 0.505–0.621‰ (I-CDES), which correspond to temperatures of 52–121°C, do not reflect Earth surface temperatures (cf., Fetrow et al., 2022). Even micritic primary samples, which did not undergo significant visible diagenetic alteration, return an average temperature of 60°C, likely due to solid-state reordering during long-term shallow burial conditions. Solid-state reordering resets clumped isotope bonds through the diffusion of C and O through the mineral lattice, changing the carbonate Δ_{47} without affecting stable isotope values or

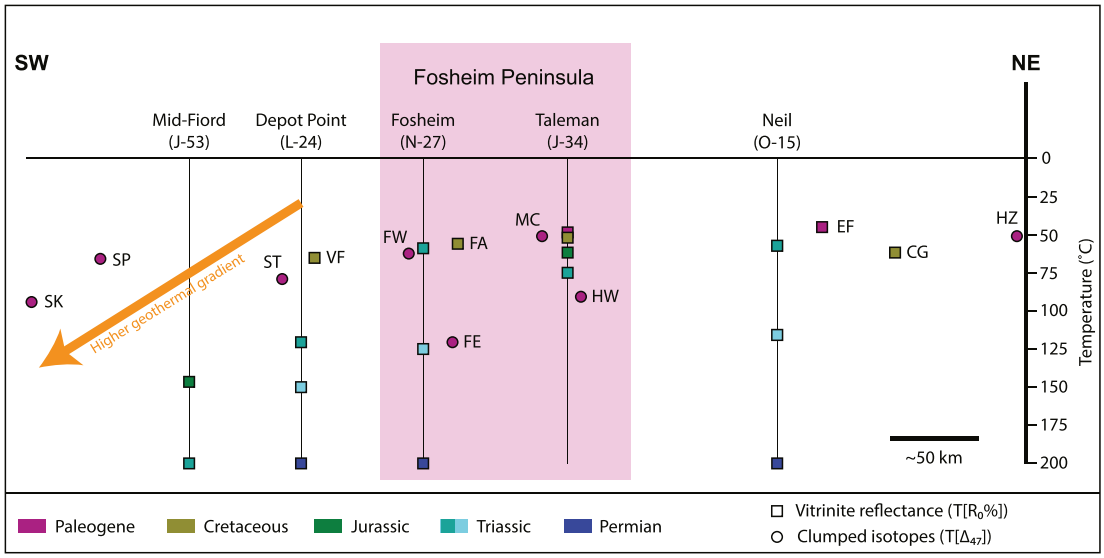

Figure 5. Spatial distribution of estimated burial temperatures across Ellesmere/Axel Heiberg Islands from vitrinite reflectance (Arne et al., 2002) and clumped isotopes (this work). Temperatures averaged for given units/ages and displayed across transect shown in Figure 1. Gray vertical lines represent well samples (names at top); other samples from outcrop (SK, Stenkul Fiord; SP, Split Lakes; ST, Strathcona Fiord; VF, Vesle Fiord; FW, Fosheim West; FE, Fosheim East; FA, Fosheim Anticline; MC, Mosquito Creek; HW, Hot Weather Creek; EF, Emma Fiord; CG, Chapman Glacier; HZ, Lake Hazen). Pink box indicates samples taken on the Fosheim Peninsula/Anticline, and orange arrow indicates region with increasing geothermal gradient (modern, assumed relict; Arne et al., 2002).

mineral texture (Henkes et al., 2014; Passey & Henkes, 2012). Our micritic sample results are consistent with low-temperature solid-state reordering, which has been shown to occur in fine-grained carbonates that experience shallow burial conditions (cf., Winkelstern & Lohmann, 2016). Winkelstern and Lohmann (2016) demonstrated that solid-state reordering of Paleogene-aged carbonates to apparent Δ_{47} temperatures of 40–75°C occurred at relatively shallow depths (1–4 km) and was not accompanied by changes to conventional carbon and oxygen isotope values, indicating greater sensitivity of Δ_{47} to burial diagenesis than stable isotopes (and also suggesting $\delta^{13}C$ and $\delta^{18}O$ record primary signals in micritic samples). Similarly, in our micritic samples, Δ_{47} values were impacted by solid-state reordering (52–67°C) during shallow burial on 10^7-year timescales, but conventional stable isotope values were unlikely to be affected by these conditions and show distinct compositions compared to known diagenetic carbonates (cf., Spar; Figure 4), suggesting they may be primary records. Shallow burial and low temperature heating of micritic samples is consistent with our knowledge of the depositional settings and preexisting thermal maturity data for ESG sediments at similar locations (e.g., Taleman Well; Figure 5). Vitrinite reflectance values from wells in ESG and related post-Cretaceous sediments from the Sverdrup Basin range from 0.3% to 0.6% (Arne et al., 2002), which corresponds to temperatures of roughly 50–75°C, consistent with the average (60°C) and range (52–67°C) of temperatures measured in our reordered micritic samples (Figure 5).

Samples that yielded temperatures higher than those likely experienced by ESG sediments during burial (>75°C, Figure 4; e.g., Arne et al., 2002; Jahren, 2007) were accompanied by visual evidence of diagenetic recrystallization (formation of calcite spar). Microspar and sparry samples have Δ_{47} values indicating formation at an average temperature of 86°C (with some samples exceeding 100°C), reflecting the formation of diagenetic spar within a previously micritic texture (Figures 3 and 4). This suggests that during relatively shallow burial of ESG sediments (<2–3 km; e.g., Ricketts & Stephenson, 1994; Arne et al., 2002), heated burial fluids from deeper units likely either modified first-generation carbonates through mineralogical recrystallization, or crystallized new coarse calcite spar in pore spaces (Alonso-Zarza, 2003; Flügel, 2010), and the Δ_{47} value (and $\delta^{13}C/\delta^{18}O$ values; see Section 5.2.1) of the resultant calcite samples records diagenetic spar temperatures and compositions (cf., Huntington et al., 2011). Variation in spar replacement temperatures may reflect variations in fluid chemistry or sediment permeability (e.g., Huntington et al., 2011), or possible proximity to faults and deformation features (e.g., Hodson et al., 2016). Spatial variations in our measured Δ_{47} temperatures of sparry samples appear to be related to the distribution of structural features in the region (Figure 5); this is likely related to differences in thermal conductivity and geothermal gradients across faults/subsurface structures (cf., Hodson et al., 2016), and to local variations in heat flow from groundwater and varying amounts of structural erosion (cf., Arne et al., 2002).

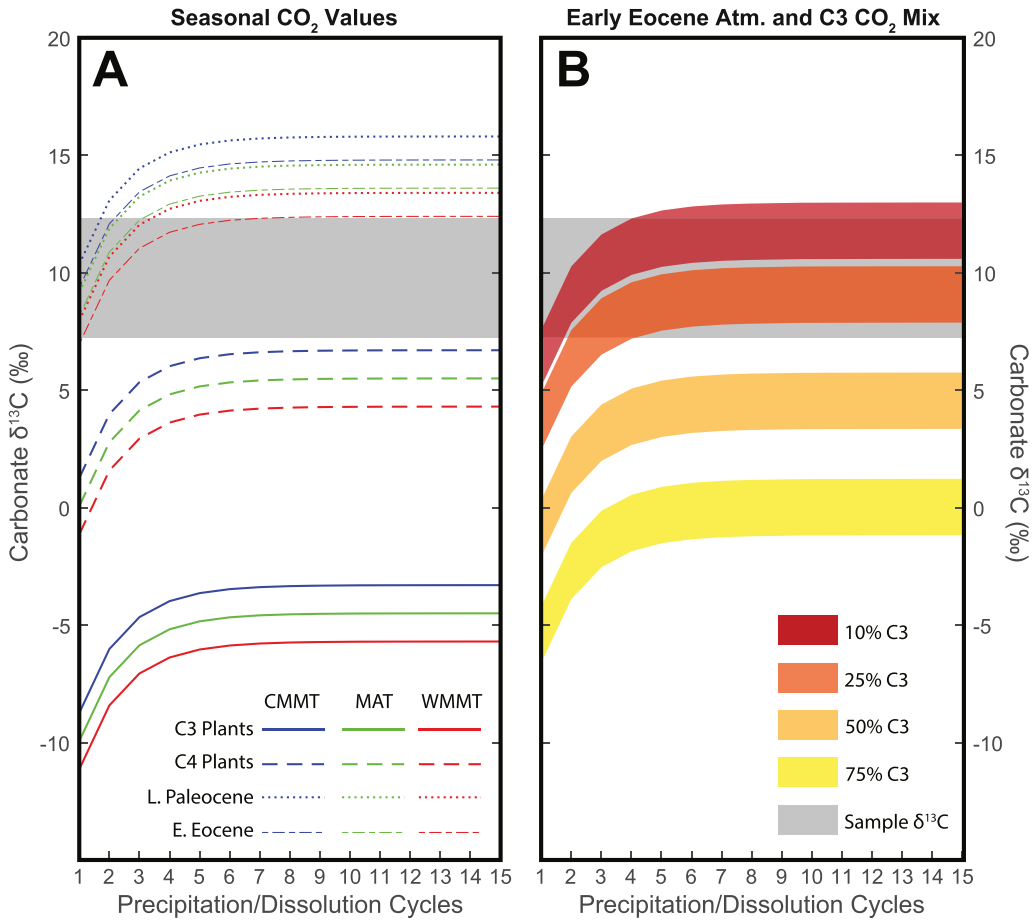

Figure 6. Carbon isotope enrichment model. (a) Evolution of carbonate $\delta^{13}C$ through repeated precipitation/dissolution cycles under cold month mean (Cold month mean temperature), mean annual (mean annual temperature), or warm month mean (warm month mean temperature) temperature conditions (see West et al., 2020), and starting with carbon from C_3 plants, C_4 plants, late Paleocene/early Eocene (P/E) atmosphere, or middle Eocene (ME) atmosphere. (b) Modeled evolution of carbonate $\delta^{13}C$ subject to repeated cycles of precipitation and dissolution, using a mix of late Paleocene/early Eocene (P/E) atmosphere and C_3 plant respired carbon. Gray shading in each panel represents range of measured carbonate $\delta^{13}C$ in our palustrine samples.

More detailed work on spar geochemistry in these and nearby localities may allow for a more precise understanding of fluid connectivity and heat flow around structural features (e.g., Fosheim Anticline) associated with ESG deposition and more recent exhumation.

5.3. Stable Isotopes and Polar Paleohydrology

5.3.1. Carbon Isotope Interpretations

Palustrine carbonate isotope signatures are generally intermediate between that of lake and soil carbonates; they are initially formed with compositions similar to that of a lacustrine carbonate, though they often exhibit lower $\delta^{13}C$ values as a result of subsequent pedogenic modification (Tandon & Andrews, 2001). For lake-setting palustrine carbonates, primary $\delta^{13}C$ values reflect the varying influences of the biogenic $\delta^{13}C$ composition (C_3 or C_4 biomass and lake productivity) and atmospheric CO_2 composition (Bernasconi & McKenzie, 2007). High microbial and algal lake productivity cause primary carbonates to have $\delta^{13}C$ values between −2 and −11‰ (Alonso-Zarza, 2003; Tandon & Andrews, 2001). Thus, the unusually positive carbon isotope values observed in our micritic samples (+7.2 to +12.3‰) and even sub-micritic samples (+2.7‰ to +6.3‰) require a mechanism that causes significant $\delta^{13}C$ enrichment in depositional settings. The most likely enrichment mechanisms, based on the location and depositional environments, are: (a) evaporative enrichment; (b) cryogenic kinetic isotope effects; (c) anoxic methanogenesis; and (d) $\delta^{13}C$ enrichment due to repeated dissolution-precipitation cycles.

Many pedogenic and lacustrine environments where carbonate is precipitated are described as closed or relatively evaporative, and evaporation under these conditions has been shown to develop carbon isotope enrichment via kinetic effects associated with concentration of the dissolved inorganic carbon pool (e.g., Horton et al., 2016; Ufnar et al., 2008). However, this process involves extreme enrichment of oxygen isotopes in these environments as well, resulting in strong covariance of $\delta^{13}C$ and $\delta^{18}O$ and high $\delta^{18}O$ values (e.g., Horton et al., 2016; Talbot, 1990). Neither of these conditions are observed here (Figure 4), suggesting that evaporative enrichment alone is insufficient to explain our carbon isotope measurements.

Cryogenic kinetic isotope effects are associated with bicarbonate dehydration from a calcium carbonate solution driven by rapid freezing of the solution and simultaneous carbonate precipitation (Burgener et al., 2018). These cryogenic kinetic isotope effects result in positive $\delta^{18}O$ and $\delta^{13}C$ anomalies and negative Δ_{47} anomalies (e.g., higher apparent carbonate formation temperatures; Burgener et al., 2018; Tripati et al., 2015). While the high $T(\Delta_{47})$ observed in our samples may be consistent with cryogenic kinetic isotope effects, the measured $\delta^{18}O$ values are not enriched relative to the expected environmental water $\delta^{18}O$ composition (see below; Jahren & Sternberg, 2008). Additionally, paleobotanical and paleontological evidence shows that our sampling locations did not experience subzero temperatures for extended periods, if at all, suggesting that the rapid freezing events required to produce cryogenic kinetic isotope effects were unlikely (e.g., Basinger et al., 1994; Dawson et al., 1993; Eberle et al., 2014; Jahren & Sternberg, 2003; West et al., 2020). Based on the relatively warm paleotemperature reconstructions and the lack of positive $\delta^{18}O$ anomalies, it seems unlikely that cryogenic kinetic isotope effects are responsible for the high primary carbonate $\delta^{13}C$ values observed in our samples.

In uniquely hypertrophic environments, anoxic methanogenesis (i.e., where methane is being produced but not oxidized) can produce significant isotopic fractionation between organic carbon and carbonates (e.g., Conrad et al., 2009; Teranes & Bernasconi, 2005). For example, Conrad et al. (2009) found carbonate $\delta^{13}C$ values of +9‰ for their samples forming in an active methanogenic environment within the anoxic zones of a hypertrophic lake. While this range of carbon isotope values is consistent with our record, this mechanism requires intense anoxia and its observation is restricted to highly organic (near-coal) layers with heavily depleted $\delta^{13}C_{org}$ values (e.g., Teranes & Bernasconi, 2005). Visual inspection of our samples suggests they are less carbon-rich than expected for sediments characteristic of anoxic methanogenesis (cf., Teranes & Bernasconi, 2005), and $\delta^{13}C_{org}$ values of bulk paludal and paleosol sediments in the Buchanan Lake Formation show no evidence for methanogenic depletion (e.g., Byrne, 2005). Therefore, while some enrichment may be possible due to hypertrophic conditions by themselves (~1–2‰; e.g., Teranes & Bernasconi, 2005), it seems unlikely that this mechanism is sufficient to produce the highly enriched carbonate $\delta^{13}C$ values observed in our sampled environments.

We suggest then that a more likely carbonate $\delta^{13}C$ enrichment mechanism is repeated dissolution/precipitation cycles, which would increase the $\delta^{13}C$ values without changing primary $\delta^{18}O$ or Δ_{47} values. Repeated cycles of carbonate dissolution and reprecipitation result in an asymptotic increase in $\delta^{13}C$ values, with the maximum $\delta^{13}C$ enrichment value controlled by the initial $\delta^{13}C$ composition of the carbonate and the temperature at which the dissolution/reprecipitation occurs (Burgener et al., 2018; Clark & Lauriol, 1992; Nakai et al., 1975). We note that this process only results in net calcite $\delta^{13}C$ enrichment if the dissolution-reprecipitation cycles occur in a closed or semi-open system with regard to the transport of CO_2 between the soil water solution and the atmosphere. Salomons and Mook (1986) showed that for carbonate reprecipitation reactions where soil pCO_2 is >0.1% atm, Rayleigh distillation (e.g., isotopic enrichment of the soil water solution due to CO_2 degassing) dominates over isotopic exchange between soil waters and the atmosphere, and the system can be considered closed. Breecker et al. (2009) showed that even in semi-arid soils (mean annual precipitation ≤550 $mmyr^{-1}$), soil pCO_2 levels can be as high as 2.6% atm, and do not typically drop below 0.13%. This suggests that the wetter, more productive palustrine environments in our study would have had sufficiently high soil pCO_2—even during the dark winter months when soil respiration rates were lower—for carbonate dissolution/reprecipitation cycles to result in net enrichment of carbonate $\delta^{13}C$ values.

To test whether this process can explain the $\delta^{13}C$ enrichment observed in our samples, we modeled the $\delta^{13}C$ evolution of carbonates subjected to repeated dissolution-reprecipitation cycles following the methods described in Burgener et al. (2018) (see also: Bottinga, 1968; Clark & Lauriol, 1992; Nakai et al., 1975). The model uses the carbon isotope fractionation factors for $CaCO_3$ and CO_2, and HCO_3^- and CO_2 (Bottinga, 1968; Mook et al., 1974), and assumed initial carbonate $\delta^{13}C$ values based on C_3 and Early Eocene atmospheric CO_2 compositions to estimate the $\delta^{13}C$ value of re-precipitated carbonate following a specified number of dissolution-precipitation events.

By accounting for enrichment, one can approximate the varying influence of plant respired and atmospheric CO_2 sources on the carbon isotope values using a two-component end member mixing model (Figure 6). End member compositions were approximated as −25‰ for C_3 vegetation, the primary vegetation type during the Eocene, and −5.9‰ for late Paleocene to early Eocene and −6.9‰ for the middle Eocene atmospheric CO_2 (Jahren & Sternberg, 2008; Schaetzl & Anderson, 2005; Tipple et al., 2010; Urban et al., 2010). Cold month mean temperature was approximated at 2˚C, MAT was approximated at 12˚C, and warm month mean temperature (WMMT) was approximated at 22˚C, based on paleobotanical methods applied to fossil leaf assemblages from these same sites (Basinger et al., 1994; Eberle et al., 2010; Greenwood & Wing, 1995; Jahren & Sternberg, 2003; Schubert et al., 2012; West et al., 2020; Wolfe, 1994). Various mixing scenarios were considered by calculating the simple weighted average between different percentages of carbonate derived from pure C_3 or pure atmospheric CO_2 (e.g., 10% C_3-derived CO_2 and 90% atmosphere-derived CO_2).

Comparing the maximum isotopic enrichment from the different temperature/CO_2 combinations indicates that the most significant influence on $\delta^{13}C$ for the samples is the specific source of the carbon incorporated into the carbonates (e.g., C_3/C_4 respired CO_2 vs. atmospheric CO_2; Figure 6). Our model results suggest that carbonates incorporating pure C_3-respired CO_2 would have final $\delta^{13}C$ values of −3.3‰ (winter precipitation/dissolution) to −5.7‰ (summer precipitation/dissolution). In contrast, carbonates incorporating only early Eocene atmospheric CO_2 would have final $\delta^{13}C$ values of 14.8‰ (winter) to 12.4‰ (summer). As shown in Figure 6, even after multiple dissolution/reprecipitation cycles, the $\delta^{13}C$ value of carbonates that incorporate only plant-respired CO_2 would still be more negative than the observed $\delta^{13}C$ values in our micritic samples. The observed level of $\delta^{13}C$ enrichment in the samples suggests that atmospheric CO_2 was the major source of carbon for these palustrine carbonates, with a relatively minor (∼10–25%) carbon input from vegetation/aquatic biomass or microbially-respired CO_2 (Figure 6b). Given the observed composition of fossil flora (e.g., West et al., 2020), the age of the ESG sediments, and the humid nature of the reconstructed environment, it is highly unlikely that C_4 or CAM plants would have been present in the region (cf., Christin & Osborne, 2014; Edwards et al., 2010); therefore, the primary source of the small amount of respired CO_2 incorporated into our carbonate samples was almost certainly derived from C_3 vegetation (cf., Figure 6).

The results of the two-component end-member mixing model place constraints on the environmental conditions during carbonate formation. Examples of dissolution-precipitation cycles resulting in $\delta^{13}C$ enrichment of this magnitude in modern environments are restricted to high latitude sites, such as Svalbard and the Antarctic Dry Valleys (e.g., Courty et al., 1994; Nakai et al., 1975). Modern carbonates formed in high latitude regions may experience this enrichment mechanism due to the pattern of continuous darkness during winter and shoulder-season months, resulting in low biological productivity and dry conditions (leading to carbonate precipitation with little or no plant-respired carbon input), followed by continuous summer sunlight associated with an influx of snowmelt flooding soils and creating ponded environments (leading to carbonate dissolution; Burgener et al., 2018). Our Eocene setting would have experienced similar light conditions that would have limited plant growth and respiration when low-light conditions would have promoted plant dormancy, and as freezing conditions were unlikely the Eocene Arctic, would not have experienced significant frost or snowmelt (Eberle & Greenwood, 2012). Studies of modern pedogenic and other terrestrial carbonates have shown that seasonal precipitation variability can affect the timing of carbonate precipitation (e.g., Breecker et al., 2009; Burgener et al., 2016; Peters et al., 2013; Quade et al., 2013; Ringham et al., 2016). Specifically, Gallagher and Sheldon (2016) suggested that in regions of highly seasonal precipitation, pedogenic carbonate formation is typically restricted to the driest time of the year (regardless of the temperature of that season), particularly when the influx of water decreases long enough to allow for supersaturation of carbonate (cf., Alonso-Zarza, 2003; Alonso-Zaraza et al., 2006). Based on these observations, we suggest that our sample $\delta^{13}C$ values and the results of our modeling experiment are most consistent with the hypothesis that during the late Paleocene to early Eocene, the Canadian Arctic hydrological regime restricted palustrine carbonate formation to the non-growing season when plant productivity was at its lowest (Figure 6), requiring a significant difference in saturation conditions between Arctic summer (growing season) and winter (period of plant respiratory dormancy) in these environments.

This suggests that the Eocene Canadian Arctic experienced some hydrological or precipitation seasonality, with more water available, or a lower evaporation-precipitation ratio, during the summer than the winter. Previous work from the Canadian Arctic established two endmember concepts for hydrological cycling during the Eocene: (a) a polar monsoon system, as indicated by summer peaks in precipitation observed in fossil wood isotopes (e.g., Schubert et al., 2012) and suggested by some model constraints (e.g., Lunt et al., 2021), and (b) an

"ever-wet" equable system, suggested as a mechanism for buffering polar warmth in other model outputs (Huber & Goldner, 2012; Kiehl & Shields, 2013) and maintaining ecosystem properties in paleontological observations (e.g., Eberle et al., 2010). However, more recent studies using climate model ensembles (e.g., Carmichael et al., 2016; Zhu et al., 2020) and comprehensive leaf physiognomy and nearest living relative analyses (e.g., West et al., 2015; West et al., 2020) have indicated that the hydrological regime of the Eocene Arctic may have been somewhat intermediate between these endmembers, where a larger proportion of precipitation is delivered in the summer months (double) and driest conditions occur during the winter/shoulder seasons (comparable to a modern/historical seasonal range; e.g., Linderholm et al., 2018; Thomas et al., 2018), without classifying as a true "monsoon" (cf., Zhang & Wang, 2008). This is supported by results from Community Earth System Model (CESM) version 1.2 as configured for the Eocene and displayed for the Arctic ($6 \times pCO_2$ simulation; Zhu et al., 2019; Zhu et al., 2020), which shows a significantly wetter Arctic (particularly >70°N) during summer months (JJA; Figures 7a and 7b).

While the Eocene Arctic was undoubtedly wetter overall than the modern/historical regime, our data are consistent with such a seasonal pattern, with winter conditions recording carbonate deposition during a drier period of the year (when palustrine environments can be super-saturated with respect to $CaCO_3$) when plants are dormant (due to temperature and/or light conditions; e.g., Basinger et al., 1994), while paired paleobotanical records from the same localities (West et al., 2015, 2020) are consistent with summer conditions recording a wetter period of the year (when carbonate dissolution occurs) when plants and soil processes are more active (due to improved temperature and light conditions). Together these records may provide a more complete picture of Eocene Arctic hydrology (cf., Carmichael et al., 2016), where summer-biased paleontological (e.g., Eberle et al., 2010) and paleobotanical (e.g., West et al., 2020) records and winter-biased isotopic records (e.g., this work) can be used together (cf., Kwiecien et al., 2022) to suggest a marked (but non-monsoonal) precipitation seasonality, which can account for seemingly disparate observations like strong isotopic signals (e.g., this work; Schubert et al., 2012) and a broad-leaved flora indicative of wet conditions (e.g., Eberle & Greenwood, 2012; Greenwood et al., 2010; West et al., 2015, 2020), as well as the presence of both palustrine coal deposits and palustrine carbonates.

5.3.2. Oxygen Isotope Source Water

Further evidence of seasonality can be derived from our carbonate $\delta^{18}O$ values, where primary $\delta^{18}O$ values in palustrine carbonates generally reflect the biogenic and temperature-dependent fractionation occurring between the calcite and original surface source water (Alonso-Zarza, 2003; Cerling & Quade, 1993; Kim & O'Neil, 1997). Evaluating the $\delta^{18}O$ of palustrine carbonates generally provides an indirect record of local rainfall and surface water (fluvial/lacustrine) inputs, and can help filter out uncertainty about hydrological dynamics, such as mixing variations or smaller seasonal changes (Bernasconi & McKenzie, 2007). Using known temperature-dependent fractionation relationships between the $\delta^{18}O$ of calcite and original source water (Alonso-Zarza, 2003; Cerling & Quade, 1993; Kim & O'Neil, 1997), we can estimate environmental water conditions.

For micritic and sub-micritic samples, we used an average estimate for CMMT of 2°C for assumed carbonate formation temperature during winter months, and an average estimate for WMMT of 20°C for assumed carbonate formation temperature during summer months (e.g., Basinger et al., 1994; Eberle et al., 2010; Greenwood & Wing, 1995; Jahren & Sternberg, 2003; Schubert et al., 2012; West et al., 2015, 2020; Wolfe, 1994). We use these paleobotanically-derived temperatures rather than our Δ_{47}-derived temperatures for this calculation because the clumped isotope values have been variably reset and therefore do not represent Earth surface temperatures (see Section 5.2.2). The converted environmental water $\delta^{18}O_{sw}$ values (VSMOW) for micritic/sub-micritic samples range from −14.3 to −17.4‰ for summer and −18.3 to −21.4‰ for winter (Figure 7). Assuming the interpretations made from the carbon isotope system are reasonable, $\delta^{18}O_{sw}$ would not be significantly impacted by biogenic fractionation. Additionally, the dissolution/reprecipitation mechanism does not inherently affect $\delta^{18}O$ (Burgener et al., 2018), so it is assumed that the $\delta^{18}O_{sw}$ values are not affected by this mechanism if the source water composition has not changed significantly during the timeframe of carbonate precipitation for a given sample (years to thousands of years; cf., Alonso-Zarza, 2003). Relatively low $\delta^{18}O_{sw}$ values are reasonable for this region and time period, because the absence of large ice sheets during the late Paleocene to middle Eocene caused global mean ocean water to have lower initial $\delta^{18}O$ values than that during times of extensive ice cover (e.g., Zachos et al., 2008), and because ^{18}O concentration decreases with increasing latitude, further reducing initial $\delta^{18}O$ in the Arctic region (Bowen, 2010; Dansgaard, 1964).

10.1029/2023PA004609

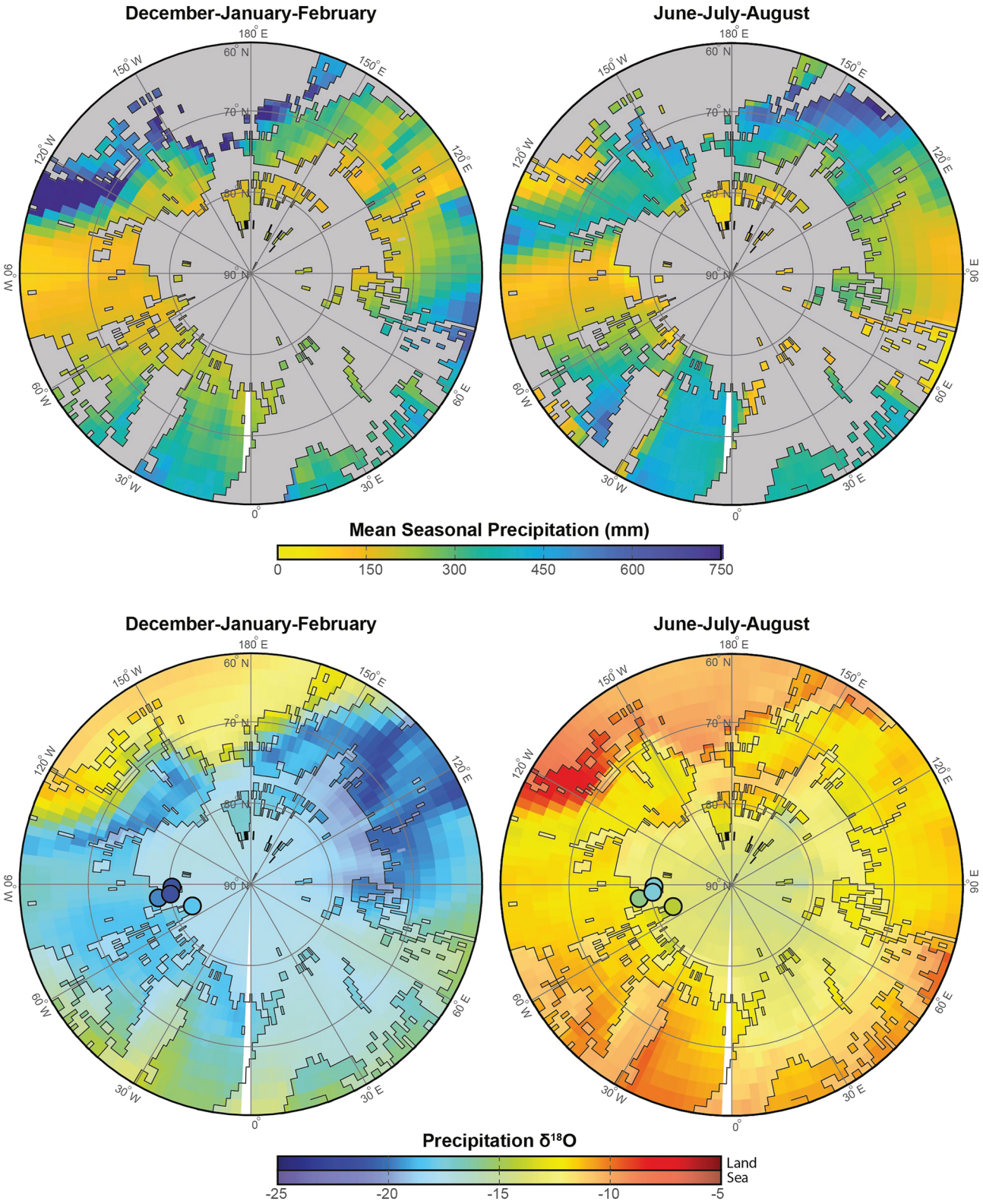

Figure 7. Isotope-enabled global climate model (iCESM1.2) simulation showing early Eocene mean seasonal precipitation results (winter, DJF; summer JJA) and $\delta^{18}O_p$ results for (winter, DJF; summer, JJA) averages ($6 \times CO_2$; Zhu et al., 2020). Proxy $\delta^{18}O_{sw}$ reconstructions from micritic samples in this study shown by colored (same scale) points.

Previous proxy estimates of environmental water $\delta^{18}O$ composition derived from fossil wood were approximated to be around −15 to −19‰ (VSMOW) on Axel Heiberg Island during the middle Eocene (Jahren & Sternberg, 2008). This range overlaps with our reconstructions of $\delta^{18}O_{sw}$ for our primary micrite samples made using either winter or summer temperatures, with theoretical winter-precipitated carbonates on the more depleted end of the range, having somewhat lower $\delta^{18}O_{sw}$ values than those recorded during a growing season (e.g., Feng et al., 2009; Jahren & Sternberg, 2008). However, newer climate models like the CESM version 1.2 have been isotope-enabled (iCESM; Brady et al., 2019) and configured for the early Eocene (e.g., Zhu et al., 2019; Zhu et al., 2020), which allows for more detailed comparison and discrimination between summer and winter proxy reconstructions. Comparing calculated winter $\delta^{18}O_{sw}$ with average modeled December-January-February (DJF) $\delta^{18}O_p$ (Figure 7c) and calculated summer $\delta^{18}O_{sw}$ with average modeled June-July-August (JJA) $\delta^{18}O_p$ (Figure 7d), we show that our proxy results align more closely with modeled winter precipitation. While we select a $6 \times CO_2$ simulation for this comparison based on fit described in previous work (Zhu et al., 2019), this conclusion holds for all available simulation scenarios (cf., Zhu et al., 2020).

Additionally, our relatively depleted $\delta^{18}O_{sw}$ values agree with previous proxy (e.g., Tripati et al., 2001; Waddell & Moore, 2008) and model (e.g., Zhu et al., 2020) reconstructions of Eocene Arctic seawater conditions suggesting a closed basin with relatively fresh surface water depleted in $\delta^{18}O$. In order to continue to explore these important facets of the paleohydrology of high latitude regions during the Paleogene, future work should focus on well-dated and precisely mapped sections in the Arctic in order to obtain higher-resolution records of hydrological changes through time (and across the region).

6. Conclusions

Stable isotope results of palustrine carbonates from ESG sediments of Ellesmere and Axel Heiberg islands provide insight into hydrological conditions at high northern latitudes during the late Paleocene to middle Eocene (~59–~45 Ma). $\delta^{13}C$ isotope values range from −4.6 to +12.3‰ Vienna-Pee Dee Belemnite (VPDB), with carbon averages of 9.8‰ for micritic (Mic), 4.5‰ for sub-micritic (SMic), 3.4‰ for microspar (MSp), and 2.0‰ for sparry (Spar) samples. $\delta^{18}O$ isotope values range from −23.1 to −15.2‰ (VPDB), with oxygen averages of −17.2‰ (Mic), −17.8‰ (SMic), −18.0‰ (MSp), −18.9‰ (Spar). $\delta^{13}C$ and $\delta^{18}O$ averages decrease with greater visual evidence of diagenetic alteration, but micritic and sub-micritic samples appear to record environmental conditions in the Eocene Arctic, which was characterized by moderate precipitation seasonality (drier winters, wetter summers) resulting in repeated dissolution/precipitation cycles for carbonate formation. Clumped isotope (Δ_{47}) values range from 0.505 to 0.621‰ (I-CDES), and micritic/sub-micritic samples (~60°C) are consistent with low temperature solid-state reordering at expected burial depths, while microspar/sparry samples (>85°C) are consistent with diagenetic spar formation controlled by emergence of deeper hydrothermal fluids possibly modulated by regional faulting/structures. Overall, this work highlights the utility of complex carbonate isotope data sets in distinguishing primary and post-burial signals, and contributes to a more complete reconstruction of the paleohydrology of the Eocene Arctic.

Conflict of Interest

The authors declare no conflicts of interest relevant to this study.

Data Availability Statement

All raw isotopic data is publicly available via the ClumpDB database from the Interdisciplinary Earth Data Alliance (IEDA) (Padgett et al., 2021).

Acknowledgments
The authors thank the University of Saskatchewan Paleobotanical Collection (USPC) for providing access to the samples, IsoLab at the University of Washington for running preliminary isotopic analyses, and Jiang Zhu for providing iCESM outputs for model comparisons. We also thank Karl Wegmann, Lonnie Leithold, Greg Tierney, and Katie Boaggio for feedback that helped improve the manuscript. Project funding came from the Geological Society of America's Graduate Student Research Grant (ABP), North Carolina State University's Graduate Student Association Research Grant (ABP), NSF Award #1813703 (EGH), and a NSERC Doctoral scholarship (CKW). Logistical and financial support for collection of samples was provided by the Natural Sciences and Engineering Research Council of Canada (IRG1334 to JFB, RGPIN2016-04337 to DRG) and the Polar Continental Shelf Project of Natural Resources Canada (to JFB).

References

Alonso-Zarza, A. M. (2003). Palaeoenvironmental significance of palustrine carbonates and calcretes in the geological record. *Earth-Science Reviews*, *60*(3), 261–298. https://doi.org/10.1016/s0012-8252(02)00106-x

Alonso-Zarza, A. M., Dorado-Valiño, M., Valdeolmillos-Rodríguez, A., & Ruiz-Zapata, M. B. (2006). A recent analogue for palustrine carbonate environments: The Quaternary deposits of las Tablas de Daimiel wetlands, Ciudad Real, Spain. *Geological Society of America Special Paper*, *416*, 153–168.

Arne, D. C., Grist, A. M., Zentilli, M., Collins, M., Embry, A., & Gentzis, T. (2002). Cooling of the Sverdrup Basin during Tertiary basin inversion: Implications for hydrocarbon exploration. *Basin Research*, *14*(2), 183–205. https://doi.org/10.1046/j.1365-2117.2002.00163.x

Basinger, J. F., Greenwood, D. R., & Sweda, T. (1994). Early Tertiary vegetation of Arctic Canada and its relevance to paleoclimatic interpretation. In M. C. Boulter & H. C. Fisher (Eds.), *Cenozoic plants and climate of the Arctic. NATO ASI series* (pp. 175–198). Springer-Verlag.

Bernasconi, S. M., Daëron, M., Bergmann, K. D., Bonifacie, M., Meckler, A. N., Affek, H. P., et al. (2021). InterCarb: A community effort to improve inter-laboratory standardization of the carbonate clumped isotope thermometer using carbonate standards. *Geochemistry, Geophysics, Geosystems*, *22*(5), e2020GC009588. https://doi.org/10.1029/2020gc009588

Bernasconi, S. M., & McKenzie, J. A. (2007). Lake sediments. *Encyclopedia of Quaternary Science*, 351–359. https://doi.org/10.1016/b0-444-52747-8/00384-7

Bottinga, Y. (1968). Calculation of fractionation factors for carbon and oxygen isotopic exchange in the system calcite-carbon dioxide-water. *Journal of Physical Chemistry*, *72*(3), 800–808. https://doi.org/10.1021/j100849a008

Bowen, G. J. (2010). Isoscapes: Spatial pattern in isotopic biogeochemistry. *Annual Review of Earth and Planetary Sciences*, *38*(1), 161–187. https://doi.org/10.1146/annurev-earth-040809-152429

Brady, E., Stevenson, S., Bailey, D., Liu, Z., Noone, D., Nusbaumer, J., et al. (2019). The connected isotopic water cycle in the Community Earth System Model version 1. *Journal of Advances in Modeling Earth Systems*, *11*(8), 2547–2566. https://doi.org/10.1029/2019ms001663

Brand, W. A., Assonov, S. S., & Coplen, T. B. (2010). Correction for the ^{17}O interference in $\delta(^{13}C)$ measurements when analyzing CO_2 with stable isotope mass spectrometry (IUPAC Technical Report). *Pure and Applied Chemistry*, *82*(8), 1719–1733. https://doi.org/10.1351/pac-rep-09-01-05

Breecker, D. O., Sharp, Z. D., & McFadden, L. D. (2009). Seasonal bias in the formation and stable isotopic composition of pedogenic carbonate in modern soils from central New Mexico, USA. *Geological Society of America Bulletin*, *121*(3–4), 630–640. https://doi.org/10.1130/b26413.1

Bristow, T. F., Bonifacie, M., Derkowski, A., Eiler, J. M., & Grotzinger, J. P. (2011). A hydrothermal origin for isotopically anomalous cap dolostone cements from south China. *Nature*, *474*(7349), 68–71. https://doi.org/10.1038/nature10096

Burgener, L., Huntington, K. W., Hoke, G. D., Schauer, A., Ringham, M. C., Latorre, C., & Díaz, F. P. (2016). Variations in soil carbonate formation and seasonal bias over > 4 km of relief in the western Andes (30 S) revealed by clumped isotope thermometry. *Earth and Planetary Science Letters*, *441*, 188–199. https://doi.org/10.1016/j.epsl.2016.02.033

Burgener, L. K., Huntington, K. W., Sletten, R., Watkins, J. M., Quade, J., & Hallet, B. (2018). Clumped isotope constraints on equilibrium carbonate formation and kinetic isotope effects in freezing soils. *Geochimica et Cosmochimica Acta*, *235*, 402–430. https://doi.org/10.1016/j.gca.2018.06.006

Byrne, M. C. (2005). A stable isotope stratigraphy for the Axel Heiberg Fossil Forest and its application to Eocene climate. (M.S. Thesis). Massachusetts Institute of Technology, Department of Earth, Atmospheric, and Planetary Sciences.

Carmichael, M. J., Lunt, D. J., Huber, M., Heinemann, M., Kiehl, J., LeGrande, A., et al. (2016). A model-model and data-model comparison for the early Eocene hydrological cycle. *Climate of the Past*, *12*(2), 455–481. https://doi.org/10.5194/cp-12-455-2016

Carpenter, R. J., Jordan, G. J., Macphail, M. K., & Hill, R. S. (2012). Near-tropical early Eocene terrestrial temperatures at the Australo-Antarctic margin, western Tasmania. *Geology*, *40*(3), 267–270. https://doi.org/10.1130/g32584.1

Cerling, T. E., & Quade, J. (1993). Climate change in continental isotopic records. *Geophysical Monograph*, *78*, 217–231.

Christin, P. A., & Osborne, C. P. (2014). The evolutionary ecology of C_4 plants. *New Phytologist*, *204*(4), 765–781. https://doi.org/10.1111/nph.13033

Clark, I. D., & Lauriol, B. (1992). Kinetic enrichment of stable isotopes in cryogenic calcites. *Chemical Geology*, *102*(1–4), 217–228. https://doi.org/10.1016/0009-2541(92)90157-z

Conrad, R., Claus, P., & Casper, P. (2009). Characterization of stable isotope fractionation during methane production in the sediment of a eutrophic lake, Lake Dagow, Germany. *Limnology & Oceanography*, *54*(2), 457–471. https://doi.org/10.4319/lo.2009.54.2.0457

Contreras, L., Pross, J., Bijl, P. K., Koutsodendris, A., Raine, J. I., van de Schootbrugge, B., & Brinkhuis, H. (2013). Early to middle Eocene vegetation dynamics at the Wilkes land margin (Antarctica). *Review of Palaeobotany and Palynology*, *197*, 119–142. https://doi.org/10.1016/j.revpalbo.2013.05.009

Courty, M. A., Marlin, C., Dever, L., Tremblay, P., & Vachier, P. (1994). The properties, genesis and environmental significance of calcitic pendants from the High Arctic (Spitsbergen). *Geoderma*, *61*(1–2), 71–102. https://doi.org/10.1016/0016-7061(94)90012-4

Daëron, M., Blamart, D., Peral, M., & Affek, H. P. (2016). Absolute isotopic abundance ratios and the accuracy of Δ_{47} measurements. *Chemical Geology*, *442*, 83–96. https://doi.org/10.1016/j.chemgeo.2016.08.014

Dansgaard, W. (1964). Stable isotopes in precipitation. *Tellus*, *16*(4), 436–468. https://doi.org/10.3402/tellusa.v16i4.8993

Dawson, M. R., McKenna, M. C., Beard, K. C., & Hutchison, J. H. (1993). An early Eocene plagiomenid mammal from Ellesmere and Axel Heiberg islands. Arctic Canada. *Kaupia*, *3*, 179–192.

Dewing, K., & Obermajer, M. (2011). Thermal maturity of the Sverdrup Basin, Arctic Canada and its bearing on hydrocarbon potential. *Geological Society, London, Memoirs*, *35*(1), 567–580. https://doi.org/10.1144/m35.38

Dewing, K., & Sanei, H. (2009). Analysis of large thermal maturity datasets: Examples from the Canadian Arctic Islands. *International Journal of Coal Geology*, *77*(3–4), 436–448. https://doi.org/10.1016/j.coal.2008.04.009

Diffenbaugh, N. S., & Field, C. B. (2013). Changes in ecologically critical terrestrial climate conditions. *Science*, *341*(6145), 486–492. https://doi.org/10.1126/science.1237123

Dunagan, S. P., & Turner, C. E. (2004). Regional paleohydrologic and paleoclimatic settings of wetland/lacustrine depositional systems in the Morrison Formation (Upper Jurassic), Western Interior, USA. *Sedimentary Geology*, *167*(3–4), 269–296. https://doi.org/10.1016/j.sedgeo.2004.01.007

Eberle, J. J., Gottfried, M. D., Hutchison, J. H., & Brochu, C. A. (2014). First record of Eocene bony fishes and crocodyliforms from Canada's Western Arctic. *PLoS One*, *9*(5), e96079. https://doi.org/10.1371/journal.pone.0096079

Eberle, J. J., Fricke, H. C., Humphrey, J. D., Hackett, L., Newbrey, M. G., & Hutchison, J. H. (2010). Seasonal variability in Arctic temperatures during early Eocene time. *Earth and Planetary Science Letters*, *296*(3–4), 481–486. https://doi.org/10.1016/j.epsl.2010.06.005

Eberle, J. J., & Greenwood, D. R. (2012). Life at the top of the greenhouse Eocene world—A review of the Eocene flora and vertebrate fauna from Canada's high Arctic. *Geological Society of America Bulletin*, *124*(1–2), 3–23. https://doi.org/10.1130/b30571.1

Eberle, J. J., & Storer, J. E. (1999). Northernmost record of brontotheres, Axel Heiberg Island, Canada—Implications for age of the Buchanan Lake Formation and brontothere paleobiology. *Journal of Paleontology*, *73*(5), 979–983. https://doi.org/10.1017/s0022336000040828

Edwards, E. J., Osborne, C. P., Stromberg, C. A. E., Smith, S. A., Bond, W. J., Christin, P. A., et al. (2010). The origins of C_4 grasslands: Integrating evolutionary and ecosystem science. *Science*, *328*(5978), 587–591. https://doi.org/10.1126/science.1177216

Eiler, J. M. (2007). "Clumped-isotope" geochemistry—The study of naturally-occurring, multiply-substituted isotopologues. *Earth and Planetary Science Letters*, *262*(3–4), 309–327. https://doi.org/10.1016/j.epsl.2007.08.020

Eiler, J. M. (2011). Paleoclimate reconstruction using carbonate clumped isotope thermometry. *Quaternary Science Reviews*, *30*(25–26), 3575–3588. https://doi.org/10.1016/j.quascirev.2011.09.001

Eldrett, J. S., Greenwood, D. R., Polling, M., Brinkhuis, H., & Sluijs, A. (2014). A seasonality trigger for carbon injection at the Paleocene–Eocene Thermal Maximum. *Climate of the Past*, *10*(2), 759–769. https://doi.org/10.5194/cp-10-759-2014

Embry, A., & Beauchamp, B. (2008). Sverdrup basin. *Sedimentary Basins of the World*, *5*, 451–471.

Estes, R., & Hutchison, J. H. (1980). Eocene lower vertebrates from Ellesmere Island, Canadian Arctic Archipelago. *Palaeogeography, Palaeoclimatology, Palaeoecology*, *30*, 325–347. https://doi.org/10.1016/0031-0182(80)90064-4

Feng, X., Faiia, A. M., & Posmentier, E. S. (2009). Seasonality of isotopes in precipitation: A global perspective. *Journal of Geophysical Research*, *114*(D8), D08116. https://doi.org/10.1029/2008jd011279

Ferry, J. M., & Gerdes, M. L. (1998). Chemically reactive fluid flow during metamorphism. *Annual Review of Earth and Planetary Sciences*, *26*(1), 255–287. https://doi.org/10.1146/annurev.earth.26.1.255

Ferry, J. M., Passey, B. H., Vasconcelos, C., & Eiler, J. M. (2011). Formation of dolomite at 40–80°C in the Latemar carbonate buildup, Dolomites, Italy, from clumped isotope thermometry. *Geology*, *39*(6), 571–574. https://doi.org/10.1130/g31845.1

Fetrow, A. C., Snell, K. E., Di Fiori, R. V., Long, S. P., & Bonde, J. W. (2022). How hot is too hot? Disentangling mid-cretaceous hothouse paleoclimate from diagenesis. *Paleoceanography and Paleoclimatology*, *37*(12), e2022PA004517. https://doi.org/10.1029/2022pa004517

Flügel, E. (2010). Diagenesis, porosity, and dolomitization. In E. Flügel (Ed.), *Microfacies of carbonate rocks: Analysis, interpretation and application* (pp. 267–338). Springer.

Francis, J. E., & Poole, I. (2002). Cretaceous and early Tertiary climates of Antarctica: Evidence from fossil wood. *Palaeogeography, Palaeoclimatology, Palaeoecology*, *182*(1–2), 47–64. https://doi.org/10.1016/s0031-0182(01)00452-7

Freytet, P. (1984). Carbonate lacustrine sediments and their transformations by emersion and pedogenesis: Importance of identifying them for paleogeographical reconstructions. *Bulletin des Centres de Recherches Exploration-Production Elf-Aquitaine*, *8*, 223–247.

Gallagher, T. M., & Sheldon, N. D. (2016). Combining soil water balance and clumped isotopes to understand the nature and timing of pedogenic carbonate formation. *Chemical Geology*, *435*, 79–91. https://doi.org/10.1016/j.chemgeo.2016.04.023

Garel, S., Schnyder, J., Jacob, J., Dupuis, C., Boussafir, M., Le Milbeau, C., et al. (2013). Paleohydrological and paleoenvironmental changes recorded in terrestrial sediments of the Paleocene-Eocene boundary (Normandy, France). *Palaeogeography, Palaeoclimatology, Palaeoecology*, *376*, 184–199. https://doi.org/10.1016/j.palaeo.2013.02.035

Grasby, S. E., & Beauchamp, B. (2008). Intrabasin variability of the carbon-isotope record across the Permian–Triassic transition, Sverdrup Basin, Arctic Canada. *Chemical Geology*, *253*(3), 141–150. https://doi.org/10.1016/j.chemgeo.2008.05.005

Greenwood, D., Basinger, J., & Smith, R. (2010). How wet was the Arctic Eocene rain forest? Estimates of precipitation from Paleogene Arctic macrofloras. *Geology*, *38*(1), 15–18. https://doi.org/10.1130/g30218.1

Greenwood, D. R., & Wing, S. L. (1995). Eocene continental climates and latitudinal temperature gradients. *Geology*, *23*(11), 1044–1048. https://doi.org/10.1130/0091-7613(1995)023<1044:eccalt>2.3.co;2

Guemas, V., Doblas-Reyes, F. J., Andreu-Burillo, I., & Asif, M. (2013). Retrospective prediction of the global warming slowdown in the past decade. *Nature Climate Change*, *3*(7), 649–653. https://doi.org/10.1038/nclimate1863

Guo, W., & Eiler, J. M. (2007). Temperatures of aqueous alteration and evidence for methane generation on the parent bodies of the CM chondrites. *Geochimica et Cosmochimica Acta*, *71*(22), 5565–5575. https://doi.org/10.1016/j.gca.2007.07.029

Harrison, J. C., Mayr, U., McNeil, D. H., Sweet, A. R., McIntyre, D. J., Eberle, J. J., et al. (1999). Correlation of Cenozoic sequences of the Canadian Arctic region and Greenland; implications for the tectonic history of northern North America. *Bulletin of Canadian Petroleum Geology*, *47*(3), 223–254.

Henkes, G. A., Passey, B. H., Grossman, E. L., Shenton, B. J., Pérez-Huerta, A., & Yancey, T. E. (2014). Temperature limits for preservation of primary calcite clumped isotope paleotemperatures. *Geochimica et Cosmochimica Acta*, *139*, 362–382. https://doi.org/10.1016/j.gca.2014.04.040

Hodson, K. R., Crider, J. G., & Huntington, K. W. (2016). Temperature and composition of carbonate cements record early structural control on cementation in a nascent deformation band fault zone: Moab Fault, Utah, USA. *Tectonophysics*, *690*, 240–252. https://doi.org/10.1016/j.tecto.2016.04.032

Hoefs, J. (2021). *Stable isotope geochemistry* (9th ed.). Springer Nature.

Horton, T. W., Defliese, W. F., Tripati, A. K., & Oze, C. (2016). Evaporation induced ^{18}O and ^{13}C enrichment in lake systems: A global perspective on hydrologic balance effects. *Quaternary Science Reviews*, *131*(B), 365–379. https://doi.org/10.1016/j.quascirev.2015.06.030

Huber, M., & Caballero, R. (2011). The early Eocene equable climate problem revisited. *Climate of the Past*, *7*(2), 603–633. https://doi.org/10.5194/cp-7-603-2011

Huber, M., & Goldner, A. (2012). Eocene monsoons. *Journal of Asian Earth Sciences*, *44*, 3–23. https://doi.org/10.1016/j.jseaes.2011.09.014

Huntington, K. W., Budd, D. A., Wernicke, B. P., & Eiler, J. M. (2011). Use of clumped-isotope thermometry to constrain the crystallization temperature of diagenetic calcite. *Journal of Sedimentary Research*, *81*(9), 656–669. https://doi.org/10.2110/jsr.2011.51

Huntington, K. W., Eiler, J. M., Affek, H. P., Guo, W., Bonifacie, M., Yeung, L. Y., et al. (2009). Methods and limitations of "clumped" CO_2 isotope (Δ_{47}) analysis by gas source isotope ratio mass spectrometry. *Journal of Mass Spectrometry*, *44*(9), 1318–1329. https://doi.org/10.1002/jms.1614

Hyland, E. G., & Sheldon, N. D. (2013). Coupled CO_2-climate response during the Early Eocene climatic optimum. *Palaeogeography, Palaeoclimatology, Palaeoecology*, *369*, 125–135. https://doi.org/10.1016/j.palaeo.2012.10.011

Hyland, E. G., Sheldon, N. D., & Cotton, J. M. (2017). Constraining the early Eocene climatic optimum: A terrestrial interhemispheric comparison. *Geological Society of America Bulletin*, *129*(1–2), 244–252. https://doi.org/10.1130/b31493.1

IPCC. (2021). In V. Masson-Delmotte, P. Zhai, A. Pirani, S. L. Connors, C. Péan, et al. (Eds.), *Climate change 2021: The physical science basis. Contribution of working group I to the sixth assessment report of the intergovernmental panel on climate change*. Cambridge University Press.

Irving, E., & Wynne, P. J. (1991). Paleomagnetic evidence for motions of parts of the Canadian Cordillera. *Tectonophysics*, *187*(1–3), 259–275. https://doi.org/10.1016/0040-1951(91)90423-p

Ivany, L. C., Brey, T., Huber, M., Buick, D. P., & Schöne, B. R. (2011). El Niño in the Eocene greenhouse recorded by fossil bivalves and wood from Antarctica. *Geophysical Research Letters*, *38*(16), L16709. https://doi.org/10.1029/2011gl048635

Jacques, F. M., Shi, G., Li, H., & Wang, W. (2014). An early–middle Eocene Antarctic summer monsoon: Evidence of "fossil climates". *Gondwana Research*, *25*(4), 1422–1428. https://doi.org/10.1016/j.gr.2012.08.007

Jahren, A. H. (2007). The Arctic forest of the middle Eocene. *Annual Review of Earth and Planetary Sciences*, *35*(1), 509–540. https://doi.org/10.1146/annurev.earth.35.031306.140125

Jahren, A. H., & Sternberg, L. S. L. (2003). Humidity estimate for the middle Eocene Arctic rain forest. *Geology*, *31*(5), 463–466. https://doi.org/10.1130/0091-7613(2003)031<0463:heftme>2.0.co;2

Jahren, A. H., & Sternberg, L. S. L. (2008). Annual patterns within tree rings of the Arctic middle Eocene (ca. 45 Ma): Isotopic signatures of precipitation, relative humidity, and deciduousness. *Geology*, *36*(2), 99–102. https://doi.org/10.1130/g23876a.1

John, C. M., & Bowen, D. (2016). Community software for challenging isotope analysis: First applications of "Easotope" to clumped isotopes. *Rapid Communications in Mass Spectrometry*, *30*(21), 2285–2300. https://doi.org/10.1002/rcm.7720

Kiehl, J. T., & Shields, C. A. (2013). Sensitivity of the Palaeocene-Eocene thermal maximum climate to cloud properties. *Philosophical Transactions of the Royal Society A*, *371*(2001), 20130093. https://doi.org/10.1098/rsta.2013.0093

Kim, S. T., & O'Neil, J. R. (1997). Equilibrium and nonequilibrium oxygen isotope effects in synthetic carbonates. *Geochimica et Cosmochimica Acta*, *61*(16), 3461–3475. https://doi.org/10.1016/s0016-7037(97)00169-5

Kraus, M. J., McInerney, F. A., Wing, S. L., Secord, R., Baczynski, A. A., & Bloch, J. (2013). Paleohydrologic response to continental warming during the Paleocene-Eocene thermal maximum, Bighorn basin, Wyoming. *Palaeogeography, Palaeoclimatology, Palaeoecology*, *370*, 196–208. https://doi.org/10.1016/j.palaeo.2012.12.008

Krishnan, S., Pagani, M., Huber, M., & Sluijs, A. (2014). High latitude hydrological changes during the Eocene thermal maximum 2. *Earth and Planetary Science Letters*, *404*, 167–177. https://doi.org/10.1016/j.epsl.2014.07.029

Kwiecien, O., Braun, T., Brunello, C. F., Faulkner, P., Hausmann, N., Helle, G., et al. (2022). What we talk about when we talk about seasonality-A transdisciplinary review. *Earth-Science Reviews*, *225*, 103843. https://doi.org/10.1016/j.earscirev.2021.103843

Linderholm, H., Nicolle, M., Francus, P., Gajewski, K., Helama, S., Korhola, A., et al. (2018). Arctic hydroclimate variability during the last 2000 years: Current understanding and research challenges. *Climate of the Past*, *14*(4), 473–514. https://doi.org/10.5194/cp-14-473-2018

Lunt, D., Bragg, F., Chan, W., Hutchinson, D., Ladant, J., Morozova, P., et al. (2021). DeepMIP: Model intercomparison of early Eocene climatic optimum (EECO) large-scale climate features and comparison with proxy data. *Climate of the Past*, *17*(1), 203–227. https://doi.org/10.5194/cp-17-203-2021

Marty, D., & Meyer, C. A. (2006). *Depositional conditions of carbonate-dominated palustrine sedimentation around the K-T boundary (faciès rognacien, northeastern pyrenean foreland, southwestern France)* (Vol. 416, pp. 169–187). Geological Society of America Special Paper.

McInerney, F. A., & Wing, S. L. (2011). The Paleocene-Eocene thermal maximum: A perturbation of carbon cycle, climate, and biosphere with implications for the future. *Annual Review of Earth and Planetary Sciences*, *39*(1), 489–516. https://doi.org/10.1146/annurev-earth-040610-133431

McIver, E. E., & Basinger, J. F. (1999). Early Tertiary floral evolution in the Canadian high Arctic. *Annals of the Missouri Botanical Garden*, *86*(2), 523–545. https://doi.org/10.2307/2666184

Miall, A. D. (1986). The Eureka sound group (upper cretaceous-Oligocene), Canadian Arctic islands. *Bulletin of Canadian Petroleum Geology*, *34*(2), 240–270.

Mix, A. C., & Ruddiman, W. F. (1984). Oxygen-isotope analyses and Pleistocene ice volumes 1. *Quaternary Research*, *21*(1), 1–20. https://doi.org/10.1016/0033-5894(84)90085-1

Mook, W. G., Bommerson, J. C., & Staverman, W. H. (1974). Carbon isotope fractionation between dissolved bicarbonate and gaseous carbon dioxide. *Earth and Planetary Science Letters*, *22*(2), 169–176. https://doi.org/10.1016/0012-821x(74)90078-8

Nakai, N., Wada, H., Kiyosu, Y., & Takimoto, M. (1975). Stable isotope of water and studies on the origin and geological history salts in the Lake Vanda area, Antarctica. *Geochemical Journal*, *9*(1), 7–24. https://doi.org/10.2343/geochemj.9.7

Núñez-Betelu, L. K., Hills, L. V., Krause, F. F., & Mclntyre, D. J. (1994). Upper cretaceous paleoshorelines of the northeastern Sverdrup Basin, Ellesmere island, Canadian Arctic Archipelago. In K. V. Simakov & D. K. Thurston (Eds.), *1994 proceedings of the international conference on Arctic margins* (pp. 43–49).

Oehlert, A. M., & Swart, P. K. (2014). Interpreting carbonate and organic carbon isotope covariance in the sedimentary record. *Nature Communications*, *5*(1), 1–7. https://doi.org/10.1038/ncomms5672

Padgett, A. B., Hyland, E. G., West, C. K., Burgener, L. B., Greenwood, D. R., & Basinger, J. F. (2021). Carbonate isotopes from the Canadian Arctic (Paleogene) [Dataset]. Interdisciplinary Earth Data Alliance (IEDA, Version 1.0). https://doi.org/10.26022/IEDA/112175

Pagani, M., Pedentchouk, N., Huber, M., Sluijs, A., Schouten, S., Brinkhuis, H., et al. (2006). Arctic hydrology during global warming at the Palaeocene/Eocene thermal maximum. *Nature*, *442*(7103), 671–674. https://doi.org/10.1038/nature05043

Parrish, J. T., Hyland, E. G., Chan, M. A., & Hasiotis, S. T. (2018). Stable and clumped isotopes in desert carbonate spring and lake deposits reveal palaeohydrology: A case study of the lower Jurassic Navajo sandstone, south-western USA. *Sedimentology*, *66*(1), 32–52. https://doi.org/10.1111/sed.12540

Passey, B. H., & Henkes, G. A. (2012). Carbonate clumped isotope bond reordering and geospeedometry. *Earth and Planetary Science Letters*, *351–352*, 223–236. https://doi.org/10.1016/j.epsl.2012.07.021

Peters, N. A., Huntington, K. W., & Hoke, G. D. (2013). Hot or not? Impact of seasonally variable soil carbonate formation on paleotemperature and O-isotope records from clumped isotope thermometry. *Earth and Planetary Science Letters*, *361*, 208–218. https://doi.org/10.1016/j.epsl.2012.10.024

Petersen, S. V., Defliese, W. F., Saenger, C., Daëron, M., Huntington, K. W., John, C. M., et al. (2019). Effects of improved ^{17}O correction on interlaboratory agreement in clumped isotope calibrations, estimates of mineral-specific offsets, and temperature dependence of acid digestion fractionation. *Geochemistry, Geophysics, Geosystems*, *20*(7), 3495–3519. https://doi.org/10.1029/2018gc008127

Pross, J., Contreras, L., Bijl, P. K., Greenwood, D. R., Bohaty, S. M., Schouten, S., et al. (2012). Persistent near-tropical warmth on the Antarctic continent during the early Eocene epoch. *Nature*, *488*(7409), 73–77. https://doi.org/10.1038/nature11300

Quade, J., Eiler, J., Daëron, M., & Achyuthan, H. (2013). The clumped isotope geothermometer in soil and paleosol carbonate. *Geochimica et Cosmochimica Acta*, *105*, 92–107. https://doi.org/10.1016/j.gca.2012.11.031

Quadrennial Defense Review Report (QDRR). (2010). *Crafting a strategic approach to climate* (p. 128). Department of Defense.

Reguero, M. A., Marenssi, S. A., & Santillana, S. N. (2002). Antarctic Peninsula and South America (Patagonia) Paleogene terrestrial faunas and environments: Biogeographic relationships. *Palaeogeography, Palaeoclimatology, Palaeoecology*, *179*(3–4), 189–210. https://doi.org/10.1016/s0031-0182(01)00417-5

Reinhardt, L., Estrada, S., Andruleit, H., Dohrmann, R., Piepjohn, K., von Gosen, W., et al. (2013). Altered volcanic ashes in Palaeocene and Eocene sediments of the Eureka sound group (Ellesmere island, Nunavut, Arctic Canada). *Zeitschrift der Deutschen Gesellschaft für Geowissenschaften*, *164*(1), 131–147. https://doi.org/10.1127/1860-1804/2013/0004

Ricketts, B. D. (1986). *New formations in the Eureka Sound group, Canadian Arctic islands* (pp. 363–374). Geological Survey of Canada. Paper 86-1B.

Ricketts, B. D., & McIntyre, D. J. (1986). *The Eureka sound group of eastern Axel Heiberg Island: New data on the Eurekan Orogeny* (pp. 405–410). Geological Survey of Canada. Paper 86-1B.

Ricketts, B. D., & Stephenson, R. A. (1994). The demise of Sverdrup Basin; Late Cretaceous-Paleogene sequence stratigraphy and forward modeling. *Journal of Sedimentary Research*, *64*(4b), 516–530.

Ringham, M. C., Hoke, G. D., Huntington, K. W., & Aranibar, J. N. (2016). Influence of vegetation type and site-to-site variability on soil carbonate clumped isotope records, Andean piedmont of Central Argentina (32–34 S). *Earth and Planetary Science Letters*, *440*, 1–11. https://doi.org/10.1016/j.epsl.2016.02.003

Ryan, W. B. F., Carbotte, S. M., Coplan, J. O., O'Hara, S., Melkonian, A., Arko, R., et al. (2009). Global multi-resolution topography synthesis. *Geochemistry, Geophysics, Geosystems*, *10*(3), Q03014. https://doi.org/10.1029/2008gc002332

Salomons, W., & Mook, W. G. (1986). Isotope geochemistry of carbonates in the weathering zone. *Handbook of Environmental Isotope Geochemistry*, *2*, 239–269.

Salpin, M., Schnyder, J., Baudin, F., Suan, G., Suc, J. P., Popsecu, S. M., et al. (2019). Evidence for suptropical warmth in the Canadian Arctic (Beaufort-Mackenzie, Northwest Territories, Canada) during the early Eocene. *Geological Society of America Special Paper*, *541*, 27.

Schaetzl, R., & Anderson, S. (2005). Soils: Genesis and geomorphology. Ch, *15*, 619–652.

Schauer, A. J., Kelson, J., Saenger, C., & Huntington, K. W. (2016). Choice of ^{17}O correction affects clumped isotope (Δ_{47}) values of CO_2 measured with mass spectrometry. *Rapid Communications in Mass Spectrometry*, *30*(24), 2607–2616. https://doi.org/10.1002/rcm.7743

Schubert, B. A., Jahren, A. H., Eberle, J. J., Sternberg, L. S. L., & Eberth, D. A. (2012). A summertime rainy season in the Arctic forests of the Eocene. *Geology*, *40*(6), 523–526. https://doi.org/10.1130/g32856.1

Sluijs, A., Schouten, S., Donders, T., Schoon, P. L., Rohl, U., Reichart, G., et al. (2009). Warm and wet conditions in the Arctic region during Eocene thermal maximum 2. *Nature Geoscience*, *2*(11), 777–780. https://doi.org/10.1038/ngeo668

Suan, G., Popescu, S. M., Suc, J. P., Schnyder, J., Fauquette, S., Baudin, F., et al. (2017). Subtropical climate conditions and mangrove growth in Arctic Siberia during the early Eocene. *Geology*, *45*(6), 539–542. https://doi.org/10.1130/g38547.1

Sudermann, M., Galloway, J. M., Greenwood, D. R., West, C. K., & Reinhardt, L. (2021). Palynostratigraphy of the lower Paleogene Margaret Formation at Stenkul Fiord, Ellesmere island, Nunavut, Canada. *Palynology*, *45*(3), 459–476. https://doi.org/10.1080/01916122.2020.1861121

Sunderlin, D., Loope, G., Parker, N. E., & Williams, C. J. (2011). Paleoclimatic and paleoecological implications of a Paleocene-Eocene fossil leaf assemblage, Chickaloon Formation, Alaska. *PALAIOS*, *26*(6), 335–345. https://doi.org/10.2110/palo.2010.p10-077r

Talbot, M. R. (1990). A review of the palaeohydrological interpretation of carbon and oxygen isotopic ratios in primary lacustrine carbonates. *Chemical Geology*, *80*(4), 261–279. https://doi.org/10.1016/0168-9622(90)90009-2

Tandon, S. K., & Andrews, J. E. (2001). Lithofacies associations and stable isotopes of palustrine and calcrete carbonates: Examples from an Indian Maastrichtian regolith. *Sedimentology*, *48*(2), 339–355. https://doi.org/10.1046/j.1365-3091.2001.00367.x

Tauxe, L., & Clark, D. R. (1987). New paleomagnetic results from the Eureka Sound group: Implications for the age of early Tertiary Arctic biota. *Geological Society of America Bulletin*, *99*(6), 739–747. https://doi.org/10.1130/0016-7606(1987)99<739:nprfte>2.0.co;2

Taylor, H. P., & Epstein, S. (1962). Relationship between $^{18}O/^{16}O$ ratios in coexisting minerals of igneous and metamorphic rocks. Part 1: Principles and experimental results. *Geological Society of America Bulletin*, *73*(4), 675. https://doi.org/10.1130/0016-7606(1962)73[675:rboric]2.0.co;2

Teranes, J. L., & Bernasconi, S. M. (2005). Factors controlling $\delta^{13}C$ values of sedimentary carbon in hypertrophic Balderggersee, Switzerland, and implications for interpreting isotope excursions in lake sedimentary records. *Limnology & Oceanography*, *50*(3), 914–922. https://doi.org/10.4319/lo.2005.50.3.0914

Thomas, E. K., Castaneda, I. S., McKay, N. P., Briner, J. P., Salacup, J. M., Nguyen, K. Q., & Schweinsberg, A. D. (2018). A wetter Arctic coincident with hemispheric warming 8,000 years ago. *Geophysical Research Letters*, *45*(19), 10637–10647. https://doi.org/10.1029/2018gl079517

Tierney, J. E., Poulsen, C. J., Montanez, I. P., Bhattacharya, T., Feng, R., Ford, H. L., et al. (2020). Past climates inform our future. *Science*, *370*(6517), 680–689. https://doi.org/10.1126/science.aay3701

Tipple, B. J., Meyers, S. R., & Pagani, M. (2010). Carbon isotope ratio of Cenozoic CO_2: A comparative evaluation of available geochemical proxies. *Paleoceanography*, *25*(3), PA3202. https://doi.org/10.1029/2009pa001851

Tripati, A., Zachos, J., Marincovich, L., & Bice, K. (2001). Late Paleocene Arctic coastal climate inferred from molluscan stable and radiogenic isotope ratios. *Palaeogeography, Palaeoclimatology, Palaeoecology*, *170*(1), 101–113. https://doi.org/10.1016/s0031-0182(01)00230-9

Tripati, A. K., Hill, P. S., Eagle, R. A., Mosenfelder, J. L., Tang, J., Schauble, E. A., et al. (2015). Beyond temperature: Clumped isotope signatures in dissolved inorganic carbon species and the influence of solution chemistry on carbonate mineral composition. *Geochimica et Cosmochimica Acta*, *166*, 344–371. https://doi.org/10.1016/j.gca.2015.06.021

Ufnar, D. F., Grocke, D. R., & Beddows, P. A. (2008). Assessing pedogenic calcite stable isotope values: Can positive linear covariant trends be used to quantify palaeo-evaporation rates? *Chemical Geology*, *256*(1–2), 46–51. https://doi.org/10.1016/j.chemgeo.2008.07.022

Uhl, D., Traiser, C., Griesser, U., & Denk, T. (2007). Fossil leaves as palaeoclimate proxies in the Palaeogene of Spitsbergen (Svalbard). *Acta Palaeobotanica*, *47*(1), 89–107.

Urban, M. A., Nelson, D. M., Jiménez-Moreno, G., Châteauneuf, J. J., Pearson, A., & Hu, F. S. (2010). Isotopic evidence of C_4 grasses in southwestern Europe during the early Oligocene–middle Miocene. *Geology*, *38*(12), 1091–1094. https://doi.org/10.1130/g31117.1

USGCRP. (2018). In D. R. Reidmiller, C. W. Avery, D. R. Easterling, K. E. Kunkel, K. L. M. Lewis, et al. (Eds.), *Impacts, risks, and adaptation in the United States: Fourth national climate assessment, volume II* (p. 1515). U.S. Global Change Research Program. https://doi.org/10.7930/NCA4.2018

von Gosen, W., Reinhardt, L., Piepjohn, K., & Schmitz, M. D. (2019). Paleogene sedimentation and Eurekan deformation in the Stenkul Fiord area of southeastern Ellesmere Island (Canadian Arctic): Evidence for a polyphase history. *Circum-Arctic Structural Events: Tectonic Evolution of the Arctic Margins and Trans-Arctic Links with Adjacent Orogens*, *541*, 325.

Waddell, L. M., & Moore, T. C. (2008). Salinity of the Eocene Arctic Ocean from oxygen isotope analysis of fish bone carbonate. *Paleoceanography*, *23*(1), PA1S12. https://doi.org/10.1029/2007pa001451

West, C. K., Greenwood, D. R., & Basinger, J. F. (2015). Was the Arctic Eocene "rainforest" monsoonal? Estimates of seasonal precipitation from early Eocene megafloras from Ellesmere island, Nunavut. *Earth and Planetary Science Letters*, *427*, 18–30. https://doi.org/10.1016/j.epsl.2015.06.036

West, C. K., Greenwood, D. R., & Basinger, J. F. (2019). The late Paleocene to early Eocene Arctic megaflora of Ellesmere and Axel Heiberg islands, Nunavut, Canada. *Palaeontographica Abteilung B*, *300*(1–6), 47–163. https://doi.org/10.1127/palb/2019/0066

West, C. K., Greenwood, D. R., Reichgelt, T., Lowe, A. J., Vachon, J. M., & Basinger, J. F. (2020). Paleobotanical proxies for early Eocene climates and ecosystems in northern North America from middle to high latitudes. *Climate of the Past*, *16*(4), 1387–1410. https://doi.org/10.5194/cp-16-1387-2020

West, R. M., Dawson, M. R., Hickey, L. J., & Miall, A. D. (1981). *Upper Cretaceous and Paleogene sedimentary rocks, eastern Canadian Arctic and related North Atlantic areas* (Vol. 7, pp. 279–298). Canadian Society of Petroleum Geologists Memoir.

West, R. M., Dawson, M. R., & Hutchison, J. H. (1977). Fossils from the Paleogene Eureka Sound formation, NWT, Canada: Occurrence, climatic and paleogeographic implications. In R. M. West (Ed.), *Paleontology and plate tectonics with special reference to the history of the Atlantic Ocean*, *Special publications in biology and geology* (Vol. 2, pp. 77–93). Milwaukee Public Museum.

Westerhold, T., Marwan, N., Drury, A., Liebrand, D., Agnini, C., Anagnostou, E., et al. (2020). An astronomically dated record of Earth's climate and its predictability over the last 66 million years. *Science*, *369*(6509), 1383–1387. https://doi.org/10.1126/science.aba6853

Willard, D., Donders, T., Reichgelt, T., Greenwood, D., Sangiorgi, F., Peterse, F., et al. (2019). Arctic vegetation, temperature, and hydrology during the Early Eocene transient global warming events. *Global and Planetary Change*, *178*, 139–152. https://doi.org/10.1016/j.gloplacha.2019.04.012

Wing, S. L., Harrington, G. J., Smith, F. A., Bloch, J. I., Boyer, D. M., & Freeman, K. H. (2005). Transient floral change and rapid global warming at the Paleocene-Eocene Boundary. *Science*, *310*(5750), 993–996. https://doi.org/10.1126/science.1116913

Winkelstern, I. Z., & Lohmann, K. C. (2016). Shallow burial alteration of dolomite and limestone clumped isotope geochemistry. *Geology*, *44*(6), 467–470. https://doi.org/10.1130/g37809.1

Wolfe, J. A. (1994). Tertiary climatic changes at middle latitudes of western North America. *Palaeogeography, Palaeoclimatology, Palaeoecology*, *108*(3–4), 195–205. https://doi.org/10.1016/0031-0182(94)90233-x

Zachos, J. C., Dickens, G. R., & Zeebe, R. E. (2008). An early Cenozoic perspective on greenhouse warming and carbon-cycle dynamics. *Nature*, *451*(7176), 279–283. https://doi.org/10.1038/nature06588

Zhang, S., & Wang, B. (2008). Global summer monsoon rainy seasons. *International Journal of Climatology*, *28*(12), 1563–1578. https://doi.org/10.1002/joc.1659

Zhu, J., Poulsen, C. J., Otto-Bliesner, B. L., Liu, Z., Brady, E. C., & Noone, D. C. (2020). Simulation of early Eocene water isotopes using an Earth system model and its implication for past climate reconstruction. *Earth and Planetary Science Letters*, *537*, 116164. https://doi.org/10.1016/j.epsl.2020.116164

Zhu, J., Poulsen, C. J., & Tierney, J. E. (2019). Simulation of Eocene extreme warmth and high climate sensitivity through cloud feedbacks. *Science Advances*, *5*(9), eaax1874. https://doi.org/10.1126/sciadv.aax1874

Zimov, S. A., Schuur, E. A., & Chapin, F. S., III. (2006). Permafrost and the global carbon budget. *Science*, *312*(5780), 1612–1613. https://doi.org/10.1126/science.1128908